Upper Respiratory Tract Resistome exhibits SARS-CoV-2 specific antimicrobial resistance patterns

Authors: Siddharth Singh Tomar[1,2] & Krishna Khairnar[1,2]*

Author Affiliation: [1]Environmental Epidemiology and Pandemic Management (EE&PM), Council of Scientific and Industrial Research-National Environmental Engineering Research Institute (CSIR-NEERI), Nagpur, India.

&

[2] Academy of Scientific and Innovative Research (AcSIR), Ghaziabad, UP, India.

*Corresponding author: Correspondence to Krishna Khairnar

e-mail: k_khairnar@neeri.res.in, kskhairnar@gmail.com

Abstract

The COVID-19 pandemic has raised concerns about antimicrobial resistance (AMR), especially in the context of secondary bacterial infections. This study investigates the impact of SARS-CoV-2 infection on the resistome of the upper respiratory tract (URT) using a metagenomic next-generation sequencing (mNGS) approach. Samples from 48 SARS-CoV-2-infected individuals and 47 healthy individuals from Central India were analyzed to assess variations in AMR gene profiles. Our results revealed significant differences in AMR gene diversity and abundance between the two groups. SARS-CoV-2 samples exhibited greater alpha diversity (Chao1 index) and higher variability, as evidenced by PCA and PCoA analyses, which showed distinct clustering. Additionally, 24 AMR gene families were significantly more abundant in the SARS-CoV-2 group. These gene families conferred resistance against 20 different drug classes, including macrolides, beta-lactams, and aminoglycosides. Notably, AMR genes linked to ESKAPE pathogens were more prevalent in the SARS-CoV-2 group. These findings highlight the potential role of SARS-CoV-2 in driving changes in the URT resistome, with implications for managing secondary infections and guiding antibiotic stewardship in future pandemics.

Keywords: *SARS-CoV-2, antimicrobial resistance, resistome, upper respiratory tract, metagenomics, ESKAPE pathogens, antibiotic resistance.*

1. Introduction

The global pandemic caused by SARS-CoV-2 has prompted extensive research on its effects beyond the immediate viral infection, particularly in the context of microbial communities and their resistomes. Understanding the resistome is crucial in understanding the broader implications of infections like COVID-19. This study focuses on the upper respiratory tract (URT) resistome and its alterations specific to SARS-CoV-2. As the URT is the primary entry point for the virus, the virus predisposes in the URT before subsequent lower respiratory tract infection, making URT an important site for exploring potential changes in antimicrobial resistance patterns among the SARS-CoV-2 infected individuals.

The URT harbors a diverse microbiome, including bacteria, fungi, and viruses; studies show that disruptions in the microbiome can lead to dysbiosis, creating an environment conducive to the selection and spread of AMR genes [1,2,3]. Several studies have demonstrated that viral infections, including those caused by influenza and other respiratory viruses, can alter microbial diversity in the respiratory tract. For example, Hanada et al. (2018) showed that Respiratory viral infections like influenza could disrupt host microbial communities and host defense, contributing to the pathogenesis of secondary bacterial infections [4]. Similarly, Tan et al. (2020) demonstrated that viral infections could induce changes in the microbiota that favor the selection of pathogenic bacteria capable of acquiring resistance [5].

AMR in the URT was a growing concern due to widespread antibiotic use in treating respiratory infections even before the COVID-19 pandemic. It was observed that antibiotic treatment can disrupt the natural balance of microbial communities, leading to the proliferation of resistant organisms [6]. Research has shown that the resistomes can serve as a reservoir for resistance factors, which could be transferred to pathogenic bacteria through horizontal gene transfer [7].

Since the onset of the COVID-19 pandemic, researchers have explored how SARS-CoV-2 infection impacts microbial communities and resistance patterns [8]. A review by Sender & Hentrich (2021) highlighted the influence of COVID-19 on the microbiome, noting that the virus-induced inflammation and immune suppression may promote bacterial growth and AMR development [9]. Furthermore, high rates of antibiotic use in COVID-19 patients have raised concerns about further promoting resistance. A World Health Organisation (WHO) statement noted that although bacterial co-infections in COVID-19 patients were relatively uncommon

(only 8%), antibiotics were widely prescribed, likely contributing to increasing AMR among affected populations [10].

Studies investigating the URT microbiome in COVID-19 patients have shown significant changes in microbial composition. Fazel et al. (2023) reported a reduction in bacterial diversity in SARS-CoV-2-infected individuals, with an increased abundance of opportunistic pathogens such as *Staphylococcus aureus* and *Pseudomonas aeruginosa*, both of which are known for their ability to acquire resistance against commonly used antibiotics[11]. A comprehensive review by Rehman (2023) concluded that the AMR genes such as *blaKPC*, *blaNDM*, *blaOXA-48* (carbapenem resistance), *mecA* (methicillin resistance), and *blaCTX-M*, *blaTEM*, *blaSHV* (ESBL production) are consistently being reported in the studies involving COVID-19 patients. These ARGs are responsible for resistance to pathogens like *Klebsiella pneumoniae*, *Acinetobacter baumannii*, *Staphylococcus aureus*, and *E. coli*.[12].

Despite the growing evidence linking SARS-CoV-2 to changes in the resistome, more research is needed to understand these interactions fully. Studies using metagenomic sequencing to profile the resistome are powerful tools for identifying AMR gene profile variations during COVID-19 infection[13]. The relationship between SARS-CoV-2 and the resistome has implications not only for COVID-19 treatment but also for broader pandemic preparedness. Understanding how viral infections influence AMR patterns will be critical for managing future outbreaks, as co-infections with resistant bacteria could complicate treatment strategies and worsen patient outcomes.

The literature review also highlights the lack of studies investigating the relationship between COVID-19 disease and changes in upper respiratory tract resistome in the Indian context. There is a comprehensive study by Nath et al. (2023) in which the authors have metagenomically investigated the changes in URT microbiome in SARS-CoV-2 infected individuals to ascertain the infection-specific signatures that may be used for developing nasal prebiotic therapies[14]. However, the authors have not investigated the paradigm of AMR alterations among the URT of SARS-CoV-2 patients.

Overall, while current research indicates that SARS-CoV-2 infection may influence microbial diversity and AMR patterns in the URT, the specific changes in the URT resistome of COVID-19 patients remain underexplored, particularly in the Indian population. This study aims to fill this gap by using a whole genome metagenomic approach to characterize the URT AMR gene

profiles within the context of SARS-CoV-2 infection. Understanding these changes could enhance the clinical management of secondary infections in COVID-19 and inform antibiotic stewardship strategies for future pandemics.

2. Materials and methods

2.1. Study Population

The samples used in the study were collected during March-April 2023. The study population belongs to the Vidarbha region of Central India, with samples collected from participants across five districts: Nagpur, Wardha, Gadchiroli, Chandrapur, and Bhandara. For the SARS-CoV-2 Negative Group (Control), the median age (interquartile range [IQR]) is 29 years (22 to 37). For the SARS-CoV-2 Positive Group, the median age (IQR) is 36 years (19 to 67). Participants from the SARS-CoV-2 group presented with severe acute respiratory infection (SARI) and/or influenza-like illness (ILI) symptoms. While the participants from the control group were asymptomatic and RTPCR negative.

2.2. Sample Collection and processing

In total, 96 URT swab samples in Viral Transport Medium (VTM) were collected for this study, out of which 48 were from SARS-CoV-2 positive patients (SARS-CoV-2 group) and 48 samples were collected from Healthy control (RTPCR negative). These samples were collected by expert healthcare professionals while following the standard sample collection guidelines. The collected samples were maintained at 4 °C ≤ 5 days (Short-term storage) and at -80 °C for the long term. Aliquots of these collected samples were then processed for SARS-CoV-2 RTPCR testing under Biosafety level-II conditions. Samples with ≤ 25 cycle threshold value of SARS-CoV-2 target genes were considered as positive samples.

2.3. DNA Extraction, Library Preparation, and Metagenomic Sequencing

DNA extraction was performed using the QIAamp DNA Microbiome Kit (Catalog No. 51704) according to the manufacturer's protocol. Following extraction, the DNA concentration was assessed with a Qubit fluorometer (ng/µL), and purity was evaluated using a Nanodrop spectrophotometer (A260/280 and A260/230 ratios). Library preparation was conducted using

the QIAseq FX DNA Library Preparation Kit[15]. Metagenomic next-generation sequencing (mNGS) was performed on the NextSeq550 platform using a 2x150 bp high-output kit, providing paired-end reads across 300 cycles.

2.4. Metagenomic Data Analysis

Metagenomic data analysis was conducted using the Chan Zuckerberg ID (CZID) web-based platform. The initial Sequencing quality control involved removing External RNA Controls Consortium (ERCC) sequences with Bowtie2 Version 2.5.4[16] and filtering out sequencing adapters, short reads, low-quality sequences, and low-complexity regions using a customized version of fastp[17]. Specifically, bases with quality scores below 17, reads shorter than 35 base pairs (bp), low-complexity sequences exceeding 40%, and sequences with more than 15 undetermined bases (Ns) were excluded.

Human sequences were filtered out through alignments with Bowtie2 and HISAT2[18] against reference human genomes. For sequences 100% identical for the first 70 bp, only one representative read was retained using CZID-dedup. The Spliced Transcripts Alignment to a Reference (STAR) algorithm[19] was also employed to remove duplicate, low-quality, and low-complexity host reads. The remaining non-human reads were aligned to the NCBI nucleotide and protein databases (NCBI Index Date: 06-02-2024) using GSNAPL and RAPSearch. After host read filtering, the remaining sequences were aligned to the NCBI nucleotide (NT) database with Minimap2[20] and the NCBI protein (NR) database with Diamond[21]. The hits from these alignments were annotated with corresponding accession numbers, and taxon counts were generated by combining results from GSNAP and RAPSearch.

Reads were de novo assembled into longer contigs using SPADES. Bowtie2 was then used to map original reads back to these contigs, restoring the link between reads and contigs. BLAST analysis was subsequently performed on the contigs against the NT-BLAST database (GSNAP) and the NR database (RAPSearch2).

2.5. AMR pipeline

CZID's AMR Pipeline v1.4.2 [22] was used for AMR analysis. AMR gene detection is performed using the Resistance Gene Identifier (RGI) tool, which aligns reads to the Comprehensive Antibiotic Resistance Database (CARD) v3.2.6 [23] to identify AMR genes and pathogen species

are determined based on these matches. Contigs are assembled using SPAdes and aligned with CARD via BLAST for further species identification. The results are reported, including detailed information on AMR genes (such as gene family and resistance mechanism), quality control metrics (e.g., the number of reads or contigs matching an AMR gene, average identity, and coverage), and pathogen-of-origin determination. Outputs from CZID's AMR Pipeline include the AMR sample report, quality-filtered reads, and contig sequences, along with raw or intermediate files for further analysis.

2.6. Statistical Analysis and Visualisation

Statistical tests and visualization of results were performed using Python 3.10.12. The analysis utilized several packages, including scipy (version 1.13.1) for t-tests and ANOVA. statsmodels (version 0.14.4) for regression models and hypothesis testing. scikit-learn (version 1.5.2) was used for PCA, PCoA, Multiple regression and additional statistical analysis. For data visualization, matplotlib (version 3.7.1) was employed, while seaborn (version 0.13.2) was used for statistical visualizations with heatmaps and violin plots. Interactive visualizations like the Sankey diagram were created using Plotly (version 5.24.1), and Data transformation tasks such as pivoting and log transformation were handled with Pandas (version 2.2.2). Basic statistical calculations were performed using numpy (version 1.26.4). The abundance metric of reads per million (RPM) was used for statistical analysis and data visualisation to normalize variations in sequencing depth across different samples.

3. Results

3.1. Summary of Sequencing Results

The SARS-CoV-2 and Control groups were subjected to metagenomic next-generation sequencing using the Illumina NextSeq550 platform. The SARS-CoV-2 sample set consists of 48 samples, with an average of 7.26 ± 1.52 million reads generated per sample. After applying Human filters (host read filters) to remove host reads, an average of 1.78 ± 0.56 million reads (25%) passed the filters. However, the control sample set consists of 47 samples, as one sample failed the quality check before sequencing, so that sample was not included in further analysis. The control group comprises 47 samples, generating an average of 6.52 ± 3.47 million reads. After applying human filters (host read filters), an average of 0.78 ± 0.37 million reads (15%) passed the filters, reflecting a considerable reduction in microbial reads post-filtering in the control data set.

3.2. Comparison of AMR Gene Alpha Diversity between SARS-CoV-2 and Control Groups

The alpha diversity analysis revealed differences in species richness between the Control and SARS-CoV-2 groups. The Chao1 index was notably higher in the SARS-CoV-2 group for $p<0.05$ (Stat = 841.00, $p = 0.0327$), indicating a broader diversity of antimicrobial resistance (AMR) genes in this group. However, the Shannon index, which accounts for both richness and evenness, showed no significant difference in alpha diversity between the groups (Stat = 1174.00, $p = 0.735$). Similarly, the Simpson index did not differ significantly (Stat = 1262.00, $p = 0.325$), suggesting that while the SARS-CoV-2 group exhibited higher species richness, the evenness of the distribution of AMR genes remained comparable to the Control group. **(Figure 1)**

3.3. PCA and PCoA Reveal Distinct Variability Between SARS-CoV-2 and Control Groups

PCA and PCoA analyses used the distance matrix the Bray-Curtis distance method generated to examine the variance and separation between SARS-CoV-2 and control groups. The first two components in the PCA explained 60.79% and 20.88% of the variance, respectively. The SARS-CoV-2 samples exhibited greater spread, indicating higher variability, while the control samples were more tightly clustered near zero, suggesting lower variance **(Figure 2).** Similarly, PCoA revealed distinct clustering, with PCoA Component 1 and Component 2 accounting for 34.50% and 15.63% of the variance **(Figure 2)**. PCA and PCoA showed significant differences between the two groups, with SARS-CoV-2 samples displaying more variability and distinct characteristics than the controls.

3.4. Bray-Curtis Dissimilarity Analysis

The Bray-Curtis dissimilarity heatmap **(Figure 3)** highlights the compositional differences between the SARS-CoV-2 samples (Sample IDs in red) and control samples (Sample IDs in blue) based on AMR gene profiles. The heatmap shows distinct clustering patterns, with SARS-CoV-2 samples exhibiting higher internal diversity (alpha diversity), as seen by the broader range of red shades. Meanwhile, control samples display more uniform blue clustering, indicating comparatively significant similarity within the group. The overall higher dissimilarity between the two groups (beta diversity) shows substantial differences in AMR gene profiles, aligning with the trends observed in the PCA and PCoA analyses.

3.5. Variations in AMR Gene Abundance Between SARS-CoV-2 and Control Groups

The Shapiro-Wilk test is used to assess whether the datasets follow a normal distribution. The results of the Shapiro-Wilk test show extremely low p-values, 4.87×10^{-111} and 2.70×10^{-93}, for the Control and SARS-CoV-2 groups, respectively. For Shapiro-Wilk test ($p > 0.05$) indicates normal distribution. **(Figure 4)** As the data was not normally distributed, a non-parametric test such as the Mann-Whitney was used instead of ANOVA. A total of 203 AMR gene families were analyzed; the Mann-Whitney ($p < 0.05$) indicated that the aggregated abundances of these certain gene families varied significantly between the two groups. However, when the thresholds for log2 fold change of ±1 along with $p < 0.05$ (Mann-Whitney) were used to visualise the relative change in average abundance of the AMR gene between two conditions (e.g., SARS-CoV-2 versus control), out of 24 genes passing the thresholds 23 AMR genes showed higher abundances in SARS-CoV-2 group, and one gene (lsa-type ABC-F protein) was more abundant in Control Group. **Table 1** Genes with a log2 fold change > 1 or < -1 and a p-value below 0.05 (above the dashed line) were marked in red. **(Figure 5)**

AMR Gene Family	log2 FC	P value	Control Aggregated Abundance	SARS-CoV-2 Aggregated Abundance	Sample Group with higher Abundance
TEM beta-lactamase	3.78	0.0001	328.95	4557.86	SARS-CoV-2
rifamycin-resistant beta-subunit of RNA polymerase (rpoB)	2.40	0.0001	303.66	1613.45	SARS-CoV-2
resistance-nodulation-cell division (RND) antibiotic efflux pump	1.91	0.0001	81.04	307.56	SARS-CoV-2
major facilitator superfamily (MFS) antibiotic efflux pump; resistance-nodulation-cell division (RND) antibiotic efflux pump	2.34	0.0001	3.77	23.23	SARS-CoV-2
major facilitator superfamily (MFS) antibiotic efflux pump	3.32	0.0001	88.76	895.84	SARS-CoV-2
ATP-binding cassette (ABC) antibiotic efflux pump; major facilitator superfamily (MFS) antibiotic efflux pump	6.74	0.0021	0.42	150.93	SARS-CoV-2
AAC(3)	5.87	0.0031	2.94	229.76	SARS-CoV-2
APH(6)	2.88	0.0091	158.33	1176.23	SARS-CoV-2
pmr phosphoethanolamine transferase	3.07	0.0101	6.56	62.86	SARS-CoV-2
kdpDE	8.56	0.0111	1.00	757.01	SARS-CoV-2
chloramphenicol acetyltransferase (CAT)	1.86	0.0121	22.92	86.08	SARS-CoV-2
fosfomycin thiol transferase	6.02	0.0131	0.78	115.19	SARS-CoV-2
ANT(4')	2.48	0.0141	0.22	5.83	SARS-CoV-2
tetracycline inactivation enzyme	2.84	0.0151	3.35	30.18	SARS-CoV-2
quinolone resistance protein (qnr)	2.65	0.0151	0.67	9.48	SARS-CoV-2
ANT(2'')	2.39	0.0201	85.68	455.26	SARS-CoV-2
ANT(3'')	4.68	0.0221	2.43	87.09	SARS-CoV-2
multidrug and toxic compound extrusion (MATE) transporter	5.79	0.0251	5.07	336.15	SARS-CoV-2
trimethoprim resistant dihydrofolate reductase dfr	3.53	0.0251	19.46	236.34	SARS-CoV-2
APH(3'')	2.73	0.0271	195.22	1304.21	SARS-CoV-2
antibiotic-resistant isoleucyl-tRNA synthetase (ileS)	2.75	0.0281	68.53	469.04	SARS-CoV-2
vga-type ABC-F protein	2.23	0.0301	1.14	9.08	SARS-CoV-2
undecaprenyl pyrophosphate related proteins	2.13	0.0301	0.59	5.96	SARS-CoV-2
lsa-type ABC-F protein	-1.49	0.0441	954.94	338.00	Control

Table 1: *Overview of AMR gene families with notable abundance differences between SARS-CoV-2 and control samples. Each entry includes the AMR gene family, log2 fold change (logFC), p-value (Mann-Whitney), aggregated abundances in both SARS-CoV-2 and Control groups and the sample group in which the gene is more abundant. Genes with logFC > 1 and p-value < 0.05 are considered significantly more abundant in SARS-CoV-2, while genes with logFC < -1 and p-value < 0.05 are considerably more abundant in controls.*

Gene families with a p-value < 0.05 (Mann-Whitney) were selected for further analysis and used to generate comparative abundance heatmaps **(Figure 6)**. The abundance values were log-

transformed (natural log) for proper visualization. The heatmaps reveal distinct AMR gene family distribution patterns, with the SARS-CoV-2 group showing a higher abundance of several AMR gene families, such as 16S rRNA methyltransferases (rmtC), ADC beta-lactamases, and General Bacterial Porins. The control group showed a lower abundance of these gene families. Some gene families, such as the MFS antibiotic efflux pump, exhibited overall moderate abundance in both groups but were still higher in the SARS-CoV-2 group.

Violin plots were used to visualize further the difference in abundance and distribution of significantly varying AMR gene families **(Figure 7)**. The SARS-CoV-2 group demonstrated higher abundances of AMR gene families such as non-erm 23S ribosomal RNA methyltransferase (G748), vga-type ABCF protein, ANT(2''), and APH(3') and APH(6) aminoglycoside resistance genes. Also, the MFS antibiotic efflux pump and TEM beta-lactamase genes were more prominent in the SARS-CoV-2 group.

When the significant AMR Gene families were further analysed for the corresponding drug class to which they may confer resistance, it was observed that these gene families were conferring resistance against the following 20 distinct drug classes, including macrolides, streptogramin, lincosamide, aminocoumarin, fluoroquinolone, tetracycline, peptide antibiotic, nitroimidazole, rifamycin, beta-lactams, pleuromutilin, aminoglycoside, disinfecting agents and antiseptics, sulfonamide, phenicol, diaminopyrimidine, nitrofuran, glycopeptides and phosphonic acid antibiotics.

3.6. Evaluation of Factors Influencing AMR Gene Abundance Using Poisson and Zero-Inflated Poisson Models

The abundance data for AMR genes was positively skewed with multiple zero values. Therefore, both Poisson regression and Zero-Inflated Poisson (ZIP) regression models were used to account for this distribution. RPM values below one were filtered out before executing the models to normalize the data and reduce noise from low-abundance observations. The Poisson model demonstrated a strong fit, with a high Pseudo R-squared of 0.9976, indicating it explained nearly all variance in AMR abundance. In contrast, the ZIP model, intended to handle excess zeros, produced a much lower Pseudo R-squared of 0.04787, with a non-significant zero-inflation component, suggesting that zero inflation did not enhance model performance for this dataset. In terms of variable effects, Sample_Type (SARS-CoV-2 vs. control) had a positive

and highly significant association with AMR abundance (coef = 0.2697, $p < 0.001$), indicating that AMR gene abundance is notably higher in the SARS-CoV-2 group. Collection_location showed a negative and significant association with AMR abundance (coef = -0.1619, $p < 0.001$), indicating that AMR gene presence varies by geographic location, with certain areas having lower levels. Host_sex was also significantly associated with the abundance of AMR genes, with a negative coefficient (coef = -0.527, $p < 0.001$), suggesting males have lower AMR gene abundance. The variable of Host_age had a small but significant negative association with AMR abundance (coef = -0.0054, $p < 0.001$), indicating a decrease in abundance with increasing age. These associations were consistent across both models, reinforcing the significance of each factor. However, the Poisson model provided a more robust fit for the data. **Table 2**

Poisson Model Summary:						
Dep. Variable:	Abundance	No. Observations:	1459			
Model:	GLM	Df Residuals:	1459			
Model Family:	Poisson	Df Model:	4			
Link Function:	Log Scale:	1				
Method:	IRLS	Log-Likelihood:	-8.77E+04			
Deviance:	1.69E+05					
No. Iterations:	6	**Pseudo R-squ. (CS):**	**0.9976**			
Covariance Type:	nonrobust					
Variable	**coef**	**std err**	**z**	**P>|z|**	**[0.025**	**0.975]**
const	4.5128	0.019	239.696	0.001	4.476	4.55
Sample_Type	0.2697	0.009	28.513	0.001	0.251	0.288
collection_location	-0.1619	0.005	-32.345	0.001	-0.172	-0.152
host_sex	-0.527	0.008	-63.693	0.001	-0.543	-0.511
host_age	-0.0054	0	-28.815	0.001	-0.006	-0.005
Zero-Inflated Poisson Model Summary:						
Dep. Variable:	Abundance	No. Observations:	1459			
Model:	ZeroInflatedPoisson	Df Residuals:	1459			
Method:	MLE	Df Model:	4			
Log-Likelihood:	-8.77E+04	**Pseudo R-squ.**	**0.04787**			
Converged:	True	LL-Null:	-9.21E+04			
Covariance Type:	nonrobust	LLR p-value:	0			
Variable	**coef**	**std err**	**z**	**P>|z|**	**[0.025**	**0.975]**
inflate_const	-20.5375	754.455	-0.027	0.981	-1499.142	1458.167
const	4.5128	0.019	239.696	0.001	4.476	4.55
Sample_Type	0.2697	0.009	28.519	0.001	0.251	0.288
collection_location	-0.1619	0.005	-32.338	0.001	-0.172	-0.152
host_sex	-0.5269	0.008	-63.682	0.001	-0.543	-0.511

host_age	-0.0054	0	-28.815	0.001	-0.006	-0.005

Table 2: *Results of the Poisson Generalized Linear Model (GLM) and the Zero-Inflated Poisson model, analyzing 1459 observations of abundance post >1 RPM filter. Key statistics include coefficients (coef), standard errors (std err), z-values, p-values (P>|z|), and confidence intervals for various independent variables (predictors), including sample type, collection location, host sex, and host age.*

3.7. The SARS-CoV-2 group showed a higher abundance of ESKAPE-associated AMR genes

The CZID AMR pipeline links AMR gene reads to their corresponding bacterial taxa, enabling visualization of variations in particular bacterial taxa and associated AMR genes. A comparative analysis of specific taxa-associated AMR genes between the SARS-CoV-2 and control groups was performed, with log-transformed abundance values of species and gene families to facilitate comparisons **(Figure 8)**. This data also facilitates the comparative analysis of the abundance of ESKAPE-associated AMR genes among the datasets. It was observed that the SARS-CoV-2 group exhibited a higher prevalence and abundance of several ESKAPE pathogens and associated AMR gene families than the control group. Abundant gene families in the SARS-CoV-2 group included 16S rRNA methyltransferases (rmtC), ADC beta-lactamases, and MFS antibiotic efflux pumps linked to pathogens such as *Klebsiella pneumoniae, Acinetobacter baumannii*, and *Pseudomonas aeruginosa*. In contrast, the control group showed lower abundances of these AMR genes across most ESKAPE pathogens. A Sankey diagram illustrates the relationship between ESKAPE pathogens and AMR gene families, with connection thickness representing RPM values **(Figure 9)**.

4. Discussion

Several studies around the globe have investigated the compositional and functional dynamics of URT microbiome in SARS-CoV-2 patients; these studies tried to explain the relationships between the URT microbiome composition and factors like disease severity, risk of developing secondary infections and utility of URT microbiome as a marker to predict disease outcomes.[24,25,26] The SARS-CoV-2 infection plays a vital role in altering the URT microbiome. However, the impact of infection on the AMR dynamics in the URT needs to be explored. Understanding the changes in AMR profiles in context with SARS-CoV-2 infection is significant for predicting secondary bacterial infection outcomes and devising effective therapeutics and management strategies for COVID-19 patients.

Stefanini et al. (2021)[27] (Hoque et al., 2021)[28] reported that SARS-CoV-2 infection is associated with higher diversity and abundance of AMR genes, suggesting a more complex microbial ecosystem or dysbiosis. Our findings also suggest that SARS-CoV-2 infection could be linked with a higher diversity and abundance of AMR genes, which could have important implications for treatment strategies and public health. The sequencing results indicated a substantial number of reads generated for both groups. However, post-filtering for human reads significantly reduced microbial reads, particularly in the control group, which may indicate a less diverse microbial community than the SARS-CoV-2 group. Post-filtering, The higher number of microbial reads in the SARS-CoV-2 samples might suggest a more complex microbial ecosystem or a potential dysbiosis due to the viral infection.

The Chao1 index demonstrated that the SARS-CoV-2 group had a greater richness of AMR gene families than the control group. This finding aligns with previous studies indicating that viral infections can influence the composition and diversity in the context of gut[29] and URT[30] microbiomes. The lack of significant differences in the Shannon and Simpson indices suggests that while the SARS-CoV-2 group have a wider variety of AMR genes, the evenness of these

distributions is similar to that of the control group, implying that the higher richness in the SARS-CoV-2 group is not associated with the skewed abundance of a few gene families.

The PCA and PCoA analysis further established the variations in AMR gene abundances between the two groups. The distinct clustering in the PCA plots indicates that the microbial communities in SARS-CoV-2 patients differ markedly from those in the control group. The tighter clustering of control samples suggests a more homogenous microbial profile, while the greater spread of the SARS-CoV-2 samples implies a wider range of microbial interactions or influences, potentially driven by the viral infection itself or subsequent antibiotic treatments.

The Bray-Curtis dissimilarity heatmap also showed internal variability in the SARS-CoV-2 samples, suggesting diverse AMR gene profiles that could be reflective of varied underlying health conditions, prior antibiotic exposure, or different environmental exposures among the patients. In contrast, the more uniform distribution among control samples highlights a less varied AMR gene landscape.

Given the non-normal distribution of the data, the Mann-Whitney test was appropriate for identifying significant variations in AMR gene families. Identifying 25 significantly varying gene families underscores the diversity in resistance mechanisms between the two groups, further implicating potential treatment challenges in the context of SARS-CoV-2 infection. A positive Log2 Fold Change indicates that a gene is more abundant or highly expressed in SARS-CoV-2 compared to control, while a negative Log2 Fold Change suggests the gene is less abundant in SARS-CoV-2 than in control. A Log2 Fold Change of 1 represents a 2-fold increase in gene abundance, whereas a Log2 Fold Change of -1 corresponds to a 2-fold decrease in abundance. After using thresholds of log2 fold change ±1 and $p < 0.05$ (Mann-Whitney), 24 AMR genes passed the applied thresholds, out of which 23 AMR genes showed higher abundance in SARS-CoV-2 samples, indicative of a potential link between SARS-CoV-2 infection and increased abundance of certain AMR genes. Only one gene, lsa-type ABC-F protein, was more abundant in the control group than the SARS-CoV-2 group. This finding points to potential changes in the resistance gene profile associated with SARS-CoV-2, potentially affecting the AMR dynamics in COVID-19 patients suffering from secondary bacterial infections. These gene families warrant further investigation, as they may contribute to the better clinical management of co-infections in COVID-19 patients.

The analysis of antimicrobial resistance (AMR) gene abundance using Poisson and Zero-Inflated Poisson (ZIP) regression models provided insights into covariates influencing AMR. The Poisson model demonstrated a high Pseudo R-squared of 0.9976, indicating it effectively explained the variance in AMR abundance, while the ZIP model's low Pseudo R-squared of 0.04787 suggested it was less suitable for this dataset. A positive association between Sample Type (SARS-CoV-2 vs. control) and AMR abundance was observed, implying that viral infections may promote certain AMR genes. Additionally, the negative association with collection location highlighted geographic variability in AMR distribution, which is indicative of higher AMR abundances linked to certain locations (Districts of Vidarbha). Gender differences and a slight decline in AMR abundance with age were also noted. Further research is needed to explore the mechanisms behind these associations and their implications for antimicrobial stewardship.

Mann-Whitney U test also revealed several AMR gene families with significantly higher abundances in the SARS-CoV-2 group. These gene families encompass diverse antimicrobial resistance (AMR) mechanisms, including ribosomal modifications by 16S rRNA methyltransferases[31] and 23S rRNA methyltransferases[32,] conferring resistance to aminoglycosides and macrolides. Beta-lactamases like NDM, OCH, SHV, and TEM degrade beta-lactam antibiotics, including carbapenems[33-36]. Efflux pumps such as ABC, MFS, and RND actively expel antibiotics, promoting multidrug resistance[37-39]. Porins reduce drug permeability, while genes like qnr and rpoB provide resistance to quinolones and rifamycins[40-42]. Resistance to tetracyclines, fosfomycin, and other antibiotics is mediated by ribosomal protection proteins, inactivation enzymes, and transferases, highlighting the complexity of AMR mechanisms[43-45].

The presence of ESKAPE-associated AMR genes in the URT microbiome showed that the SARS-CoV-2 group harboured a higher prevalence and abundance of these clinically relevant pathogens. The enrichment of AMR genes linked to ESKAPE pathogens, known for their high resistance and clinical significance, underscores the urgent need for effective antimicrobial stewardship and infection control measures, particularly in SARS-CoV-2 patients who may be at higher risk for secondary infections.

The analysis of AMR genes in the SARS-CoV-2 samples reveals significant resistance across multiple antibiotic drug classes. Resistance to macrolides, streptogramins, and lincosamides, which are commonly used for treating gram-positive infections[46], could complicate treatment strategies for commonly occurring respiratory gram-positive infections. The detection of

resistance genes to broad-spectrum antibiotics, such as fluoroquinolones, tetracyclines, and beta-lactams, raises concerns about their limited efficacy, particularly in hospital settings where multidrug-resistant organisms are prevalent. The presence of peptide and glycopeptide resistance genes in the URT resistome, which includes resistance to last-resort antibiotics like colistin and vancomycin, was also observed among the samples. Additionally, resistance to nitroimidazoles, rifamycins, aminoglycosides, and pleuromutilins suggests that even alternative therapies may face reduced effectiveness in case of drug-resistant infection[47]. The identification of resistance to sulfonamides, phenicols, and nitrofurans points towards continuous and indiscriminate antibiotics, leading to reduced efficacy of these drug classes among the studied population. Moreover, resistance genes related to disinfecting agents and antiseptics highlight potential challenges in infection control within healthcare environments. Overall, these findings emphasize the need for robust AMR surveillance and antibiotic stewardship in the context of the COVID-19 pandemic, where bacterial co-infections in vulnerable patients may limit treatment options and contribute to the spread of resistant strains.

The increased diversity and abundance of AMR genes in SARS-CoV-2 patients could have significant implications for treatment protocols, necessitating a reassessment of antibiotic usage protocols, especially during viral infections like Influenza or SARS-CoV-2. Moreover, the identified gene families could serve as a data point to develop decision support systems for treating AMR in the context of COVID-19.

Further research is warranted to explore the clinical consequences of the observed AMR gene profiles, including the impact on treatment outcomes and the role of the URT microbiome in modulating host responses to SARS-CoV-2 infection. Longitudinal studies are needed to track changes in AMR gene abundance over time and assess the potential effects of various factors, including factors governing co-morbidities, degree of disease severity and antibiotic treatments.

In conclusion, the distinct AMR gene profiles observed in the SARS-CoV-2 group emphasize the need for ongoing surveillance and targeted interventions to mitigate the risks associated with antimicrobial resistance in the context of viral infections.

Limitations of the Study

The cross-sectional study design limits the ability to understand temporal changes in AMR gene profiles. Additionally, the potential impacts of antibiotic usage on AMR profiles could not be assessed in this study, as this is a retrospective study and antibiotic usage data were not

collected when the samples were originally obtained for SARS-CoV-2 genome surveillance under the INSACOG mandate. Furthermore, the ZIP regression model explained only a small portion of the variance observed in the data, indicating the presence of some unmeasured confounders. Future research could enhance the robustness of the findings.

***

Figure Legends

Figure 1: Overall Chao1, Shannon, and Simpson Diversity of AMR Genes: Chao1 diversity (left), Shannon diversity (center), and Simpson diversity (right) all display a greater range of diversity in the SARS-CoV-2 group, with statistically significant differences in Chao1 diversity ($p < 0.01$)

Figure 2: PCA and PCoA plots using the Bray-Curtis distance: The top plot represents the PCA (Principal Component Analysis) plot for SARS-CoV-2 and Control data, highlighting the variance explained by the first two components. SARS-CoV-2 samples are marked in red, and Control samples in blue. The bottom plot shows the PCoA (Principal Coordinates Analysis) of the same data, where the variation between the two groups is visualized across two primary axes, PC 1 and PC 2.

Figure 3: Bray-Curtis Dissimilarity Heatmap: This heatmap represents the pairwise dissimilarity between the SARS-CoV-2 samples (Sample IDs in red) and control samples (Sample IDs in blue) using the Bray-Curtis metric. Samples with similar microbial compositions are closer to blue, while highly dissimilar samples are represented in red. The diagonal represents perfect similarity (self-comparison), indicated in dark blue.

Figure 4: Normality Distribution of SARS-CoV-2 and Control Group (Histogram and QQ plots): The figure shows the abundance distribution for two groups: a control group (top row) and a SARS-CoV-2 group (bottom row). The left panels are histograms illustrating the skewed

abundance data, while the right panels are Q-Q plots, highlighting deviations from normality, with significant tails on the right-hand side, indicating non-normal distributions in both groups.

Figure 5: Volcano plot of AMR gene family abundance changes between SARS-CoV-2 and control samples, based on a Mann-Whitney U test. The x-axis represents log2 fold change (positive for SARS-CoV-2, negative for control), and the y-axis shows -log10 p-values, with higher values indicating statistical significance. Points above the dashed line at -log10(0.05) are significant ($p < 0.05$). Gene families with |log2 fold change| > 1 and p-value < 0.05 are highlighted in red, indicating significant abundance changes between the two groups.

Figure 6: Compositional Variations in the abundance of AMR gene families among Control and SARS-CoV-2 groups (Log-Transformed Significant Genes): The heatmaps illustrate the log-transformed abundance of significant AMR (antimicrobial resistance) genes across two groups: Control (top) and SARS-CoV-2 (bottom). Each row represents a distinct gene family, and each column represents a sample. The color intensity reflects gene abundance, with darker colors indicating higher abundance. The heatmaps provide a comparative visualization, highlighting compositional variations between the two groups.

Figure 7: Violin Plots of Significant AMR Gene Families (p-value < 0.05) Violin plots display the distribution of abundance for various AMR gene families that show significant differences ($p < 0.05$) between Control (blue) and SARS-CoV-2 (red) groups. Each plot corresponds to a specific gene family, with the y-axis representing abundance and the x-axis representing the sample group. The plots highlight the central tendency, variability, and distribution shape of gene abundance, emphasizing differences in AMR gene composition between the groups.

Figure 8: Variations in the Abundance of ESKAPE-associated AMR Genes Among Control and SARS-CoV-2 Groups (Log-Transformed) The heatmaps display log-transformed read counts per million (RPM) of ESKAPE-associated species and AMR gene families in the Control (top) and SARS-CoV-2 (bottom) groups. The intensity of the color represents the abundance, with darker shades indicating the higher abundance of specific AMR gene families across species in each group.

Figure 9: Sankey Diagram Showing the Relationship Between Read Species and AMR Gene Families in SARS-CoV-2 and Control Groups This Sankey diagram illustrates the connections

between bacterial species and their associated antimicrobial resistance (AMR) gene families in both SARS-CoV-2 and Control groups. The width of the flows between species and gene families indicates the abundance in RPM.

Data availability statement

The data is available as supplementary data with the file name "**combined_supplementary_data**" Any additional data, if required, will be made available on request by the authors.

Author declaration

The authors assure that the research has followed all ethical guidelines and received approvals from the Institutional Ethics Committee for Research on Human Subjects (IEC) of CSIR-NEERI, Nagpur-20, India. Necessary consent from patients/participants has been obtained, and relevant institutional documentation has been archived.

Confidentiality declaration

Sample IDs (23G214-5G-264_S1 to 23G214-5G-311_S48 and 24D214-5G_387_S45 to 24D214-5G_434_S91) are masked IDs and cannot be traced to participant details. The precise age of the participants is masked, and non-overlapping age ranges were used.

Author contribution statement

SST and KK have contributed equally to the conceptualization, experimentation, and data analysis of this study.

Conflict of interest statement

The authors declare no conflict of interest

Acknowledgement

The authors are thankful to CSIR-NEERI for providing funds under project OLP-57 (March 2023 -April 2024) for conducting this study. This manuscript has obtained the approval of the Knowledge Resource Center (KRC) publication committee of CSIR-NEERI

(KRC No.: CSIR-NEERI/KRC/2024/NOV/EEPM/1) Date: 14-11-2024

References

1. Ramamurthy, T., Ghosh, A., Chowdhury, G., Mukhopadhyay, A. K., Dutta, S., & Miyoshi, S. (2022). Deciphering the genetic network and programmed regulation of antimicrobial resistance in bacterial pathogens. Frontiers in Cellular and Infection Microbiology, 12, 952491. https://doi.org/10.3389/fcimb.2022.952491
2. Kessler, C., Hou, J., Neo, O., & Buckner, M. (2022). In situ, in vivo, and in vitro approaches for studying AMR plasmid conjugation in the gut microbiome. FEMS Microbiology Reviews, 47. https://doi.org/10.1093/femsre/fuac044.
3. Boerlin, P., & Reid-Smith, R. (2008). Antimicrobial resistance: its emergence and transmission. Animal Health Research Reviews, 9, 115 - 126. https://doi.org/10.1017/S146625230800159X.
4. Hanada, S., Pirzadeh, M., Carver, K., & Deng, J. (2018). Respiratory Viral Infection-Induced Microbiome Alterations and Secondary Bacterial Pneumonia. Frontiers in Immunology, 9. https://doi.org/10.3389/fimmu.2018.02640.
5. Tan, K., Lim, R., Liu, J., Ong, H., Tan, V., Lim, H., Chung, K., Adcock, I., Chow, V., & Wang, D. (2020). Respiratory Viral Infections in Exacerbation of Chronic Airway Inflammatory Diseases: Novel Mechanisms and Insights From the Upper Airway Epithelium. Frontiers in Cell and Developmental Biology, 8. https://doi.org/10.3389/fcell.2020.00099.
6. Bottery, M., Pitchford, J., & Friman, V. (2020). Ecology and evolution of antimicrobial resistance in bacterial communities. The ISME Journal, 15, 939 - 948. https://doi.org/10.1038/s41396-020-00832-7.
7. Despotovic, M., De Nies, L., Busi, S. B., & Wilmes, P. (2023). Reservoirs of antimicrobial resistance in the context of One Health. Current Opinion in Microbiology, 73, 102291. https://doi.org/10.1016/j.mib.2023.102291

8. Segala, F. V., Bavaro, D. F., Di Gennaro, F., Salvati, F., Marotta, C., Saracino, A., Murri, R., & Fantoni, M. (2021). Impact of SARS-CoV-2 Epidemic on Antimicrobial Resistance: A Literature Review. Viruses, 13(11), 2110. https://doi.org/10.3390/v13112110
9. Sender, V., & Hentrich, K. (2021). Virus-Induced Changes of the Respiratory Tract Environment Promote Secondary Infections With Streptococcus pneumoniae. Frontiers in Cellular and Infection Microbiology, 11, 643326. https://doi.org/10.3389/fcimb.2021.643326
10. World Health Organization: WHO. (2024, April 26). WHO reports widespread overuse of antibiotics in patients hospitalized with COVID-19. World Health Organization. https://www.who.int/news/item/26-04-2024-who-reports-widespread-overuse-of-antibiotics-in-patients--hospitalized-with-covid-19#:~:text=Highest%20rate%20of%20antibiotic%20use,the%20African%20Region%20(79%25).
11. Fazel, P., Sedighian, H., Behzadi, E., Kachuei, R., & Fooladi, A. a. I. (2023). Interaction between SARS-COV-2 and pathogenic bacteria. Current Microbiology, 80(7). https://doi.org/10.1007/s00284-023-03315-y
12. Rehman, S. (2023). A parallel and silent emerging pandemic: Antimicrobial resistance (AMR) amid COVID-19 pandemic. Journal of Infection and Public Health, 16(4), 611–617. https://doi.org/10.1016/j.jiph.2023.02.021
13. Mac Aogáin, M., Lau, K. J. X., Cai, Z., Narayana, J. K., Purbojati, R. W., Drautz-Moses, D. I., Gaultier, N. E., Jaggi, T. K., Tiew, P. Y., Ong, T. H., Koh, M. S., Hou, A. L. Y., Abisheganaden, J. A., Tsaneva-Atanasova, K., Schuster, S. C., & Chotirmall, S. H. (2020). Metagenomics reveals a core macrolide resistome related to microbiota in chronic respiratory disease. American Journal of Respiratory and Critical Care Medicine, 202(3), 433–447. https://doi.org/10.1164/rccm.201911-2202oc
14. Nath, S., Sarkar, M., Maddheshiya, A., De, D., Paul, S., Dey, S., Pal, K., Roy, S. K., Ghosh, A., Sengupta, S., Paine, S. K., Biswas, N. K., Basu, A., & Mukherjee, S. (2023). Upper respiratory tract microbiome profiles in SARS-CoV-2 Delta and Omicron infected patients exhibit variant specific patterns and robust prediction of disease groups. Microbiology Spectrum, 11(6). https://doi.org/10.1128/spectrum.02368-23
15. QIASEq FX DNA Library Kit. (2023). Qiagen.com. https://www.qiagen.com/zh-us/products/discovery-and-translational-research/next-generation-sequencing/metagenomics/qiaseq-fx-dna-library-kit
16. Langmead, B., & Salzberg, S. L. (2012). Fast gapped-read alignment with Bowtie 2. Nature Methods, 9(4), 357-359. https://doi.org/10.1038/nmeth.1923
17. Chen, S. (2023). Ultrafast one-pass FASTQ data preprocessing, quality control, and deduplication using fastp. IMeta, 2(2), e107. https://doi.org/10.1002/imt2.107

18. Kim, D., Paggi, J. M., Park, C., Bennett, C., & Salzberg, S. L. (2019). Graph-based genome alignment and genotyping with HISAT2 and HISAT-genotype. Nature Biotechnology, 37(8), 907-915. https://doi.org/10.1038/s41587-019-0201-4
19. Dobin, A., Davis, C. A., Schlesinger, F., Drenkow, J., Zaleski, C., Jha, S., Batut, P., Chaisson, M., & Gingeras, T. R. (2012). STAR: ultrafast universal RNA-seq aligner. Bioinformatics, 29(1), 15–21. https://doi.org/10.1093/bioinformatics/bts635
20. Li, H. (2018). Minimap2: Pairwise alignment for nucleotide sequences. Bioinformatics, 34(18), 3094-3100. https://doi.org/10.1093/bioinformatics/bty191
21. Buchfink, B., Xie, C., & Huson, D. H. (2014). Fast and sensitive protein alignment using DIAMOND. Nature Methods, 12(1), 59-60. https://doi.org/10.1038/nmeth.3176
22. Langelier, C., Lu, D., Kalantar, K., Chu, V., Glascock, A., Guerrero, E., Bernick, N., Butcher, X., Ewing, K., Fahsbender, E., Holmes, O., Hoops, E., Jones, A., Lim, R., McCanny, S., Reynoso, L., Rosario, K., Tang, J., Valenzuela, O., . . . McArthur, A. (2024). Simultaneous detection of pathogens and antimicrobial resistance genes with the open source, cloud-based, CZ ID pipeline. Research Square (Research Square). https://doi.org/10.21203/rs.3.rs-4271356/v1
23. Alcock, B. P., Huynh, W., Chalil, R., Smith, K. W., Raphenya, A. R., Wlodarski, M. A., Edalatmand, A., Petkau, A., Syed, S. A., Tsang, K. K., Baker, S. J. C., Dave, M., McCarthy, M. C., Mukiri, K. M., Nasir, J. A., Golbon, B., Imtiaz, H., Jiang, X., Kaur, K., . . . McArthur, A. G. (2022). CARD 2023: expanded curation, support for machine learning, and resistome prediction at the Comprehensive Antibiotic Resistance Database. Nucleic Acids Research, 51(D1), D690–D699. https://doi.org/10.1093/nar/gkac920
24. De Maio, F., Posteraro, B., Ponziani, F. R., Cattani, P., Gasbarrini, A., & Sanguinetti, M. (2020). Nasopharyngeal microbiota profiling of SARS-COV-2 infected patients. Biological Procedures Online, 22(1). https://doi.org/10.1186/s12575-020-00131-7
25. **Rhoades**, N. S., Pinski, A. N., Monsibais, A. N., Jankeel, A., Doratt, B. M., Cinco, I. R., Ibraim, I., & Messaoudi, I. (2021). Acute SARS-CoV-2 infection is associated with an increased abundance of bacterial pathogens, including Pseudomonas aeruginosa in the nose. Cell Reports, 36(9), 109637. https://doi.org/10.1016/j.celrep.2021.109637
26. Ventero, M. P., Moreno-Perez, O., Molina-Pardines, C., Paytuví-Gallart, A., Boix, V., Escribano, I., Galan, I., González-delaAleja, P., López-Pérez, M., Sánchez-Martínez, R., Merino, E., & Rodríguez, J. C. (2022). Nasopharyngeal Microbiota as an early severity biomarker in COVID-19 hospitalised patients. Journal of Infection, 84(3), 329-336. https://doi.org/10.1016/j.jinf.2021.12.030
27. Stefanini, I., De Renzi, G., Foddai, E., Cordani, E., & Mognetti, B. (2021). Profile of Bacterial Infections in COVID-19 Patients: Antimicrobial Resistance in the Time of SARS-CoV-2. Biology, 10(9), 822. https://doi.org/10.3390/biology10090822

28. Hoque, M. N., Sarkar, M. M., Rahman, M. S., Akter, S., Banu, T. A., Goswami, B., Jahan, I., Hossain, M. S., Shamsuzzaman, A. K., Nafisa, T., Molla, M. M., Yeasmin, M., Ghosh, A. K., Osman, E., Alam, S. K., Uzzaman, M. S., Habib, M. A., Mahmud, A. S., Crandall, K. A., . . . Khan, M. S. (2021). SARS-CoV-2 infection reduces human nasopharyngeal commensal microbiome with inclusion of pathobionts. Scientific Reports, 11(1), 1-17. https://doi.org/10.1038/s41598-021-03245-4
29. Li, J., Jing, Q., Li, J., Hua, M., Di, L., Song, C., Huang, Y., Wang, J., Chen, C., & Wu, A. R. (2023). Assessment of microbiota in the gut and upper respiratory tract associated with SARS-CoV-2 infection. Microbiome, 11(1). https://doi.org/10.1186/s40168-022-01447-0
30. Shilts, M. H., Rosas-Salazar, C., Strickland, B. A., Kimura, K. S., Asad, M., Sehanobish, E., Freeman, M. H., Wessinger, B. C., Gupta, V., Brown, H. M., Boone, H. H., Patel, V., Barbi, M., Bottalico, D., O'Neill, M., Akbar, N., Rajagopala, S. V., Mallal, S., Phillips, E., . . . Das, S. R. (2022). Severe COVID-19 is associated with an altered upper respiratory tract microbiome. Frontiers in Cellular and Infection Microbiology, 11. https://doi.org/10.3389/fcimb.2021.781968
31. Zarubica, T., Baker, M. R., Wright, H. T., & Rife, J. P. (2010). The aminoglycoside resistance methyltransferases from the ArmA/Rmt family operate late in the 30S ribosomal biogenesis pathway. RNA, 17(2), 346–355. https://doi.org/10.1261/rna.2314311
32. Park, A. K., Kim, H., & Jin, H. J. (2010). Phylogenetic analysis of rRNA methyltransferases, Erm and KsgA, as related to antibiotic resistance. FEMS Microbiology Letters, no. https://doi.org/10.1111/j.1574-6968.2010.02031.x
33. Kumarasamy, K. K., Toleman, M. A., Walsh, T. R., Bagaria, J., Butt, F., Balakrishnan, R., Chaudhary, U., Doumith, M., Giske, C. G., Irfan, S., Krishnan, P., Kumar, A. V., Maharjan, S., Mushtaq, S., Noorie, T., Paterson, D. L., Pearson, A., Perry, C., Pike, R., . . . Woodford, N. (2010). Emergence of a new antibiotic resistance mechanism in India, Pakistan, and the UK: a molecular, biological, and epidemiological study. The Lancet Infectious Diseases, 10(9), 597–602. https://doi.org/10.1016/s1473-3099(10)70143-2
34. Nadjar, D., Labia, R., Cerceau, C., Bizet, C., Philippon, A., & Arlet, G. (2001). Molecular Characterization of Chromosomal Class C β-Lactamase and Its Regulatory Gene in Ochrobactrum anthropi. Antimicrobial Agents and Chemotherapy, 45(8), 2324–2330. https://doi.org/10.1128/aac.45.8.2324-2330.2001
35. Bradford, P. A. (2001). Extended-Spectrum Β-Lactamases in the 21st Century: Characterization, Epidemiology, and detection of this important resistance threat. Clinical Microbiology Reviews, 14(4), 933–951. https://doi.org/10.1128/cmr.14.4.933-951.2001
36. Bradford, P. A. (2001). Extended-Spectrum Β-Lactamases in the 21st Century: Characterization, Epidemiology, and detection of this important resistance threat. Clinical Microbiology Reviews, 14(4), 933–951. https://doi.org/10.1128/cmr.14.4.933-951.2001

37. Fath, M. J., & Kolter, R. (1993). ABC transporters: bacterial exporters. Microbiological Reviews, 57(4), 995–1017. https://doi.org/10.1128/mr.57.4.995-1017.1993
38. Li, X., & Nikaido, H. (2009). Efflux-Mediated Drug Resistance in bacteria. Drugs, 69(12), 1555–1623. https://doi.org/10.2165/11317030-000000000-00000
39. Blair, J. M., & Piddock, L. J. (2009). Structure, function and inhibition of RND efflux pumps in Gram-negative bacteria: an update. Current Opinion in Microbiology, 12(5), 512–519. https://doi.org/10.1016/j.mib.2009.07.003
40. Wright, A. G. M. G. D. (2024). The Comprehensive Antibiotic Resistance Database General Bacterial porin with reduced permeability to beta-lactams. Retrieved October 23, 2024, from https://card.mcmaster.ca/ontology/41445
41. Wang, M., Guo, Q., Xu, X., Wang, X., Ye, X., Wu, S., Hooper, D. C., & Wang, M. (2009). New Plasmid-Mediated Quinolone Resistance Gene, qnrC , Found in a Clinical Isolate of Proteus mirabilis. Antimicrobial Agents and Chemotherapy, 53(5), 1892–1897. https://doi.org/10.1128/aac.01400-08
42. Ingham, C. J., & Furneaux, P. A. (2000). Mutations in the β subunit of the Bacillus subtilis RNA polymerase that confer both rifampicin resistance and hypersensitivity to NusG. Microbiology, 146(12), 3041–3049. https://doi.org/10.1099/00221287-146-12-3041
43. Wright, A. G. M. G. D. (2024). The Comprehensive Antibiotic Resistance Database tetracycline-resistant ribosomal protection protein. Retrieved October 23, 2024, from https://card.mcmaster.ca/ontology/35921
44. Nguyen, F., Starosta, A. L., Arenz, S., Sohmen, D., Dönhöfer, A., & Wilson, D. N. (2014). Tetracycline antibiotics and resistance mechanisms. Biological Chemistry, 395(5), 559–575. https://doi.org/10.1515/hsz-2013-0292
45. Rigsby, R. E., Rife, C. L., Fillgrove, K. L., Newcomer, M. E., & Armstrong, R. N. (2004). Phosphonoformate: a minimal transition state analogue inhibitor of the fosfomycin resistance protein, FOSA,. Biochemistry, 43(43), 13666–13673. https://doi.org/10.1021/bi048767h
46. Lim, J., Kwon, A., Kim, S., Chong, Y., Lee, K., & Choi, E. (2002). Prevalence of resistance to macrolide, lincosamide and streptogramin antibiotics in Gram-positive cocci isolated in a Korean hospital.. The Journal of antimicrobial chemotherapy, 49 3, 489-95 . https://doi.org/10.1093/JAC/49.3.489.
47. Guardabassi, L., & Courvalin, P. Modes of Antimicrobial Action and Mechanisms of Bacterial Resistance. 1-18. https://doi.org/10.1128/9781555817534.ch1

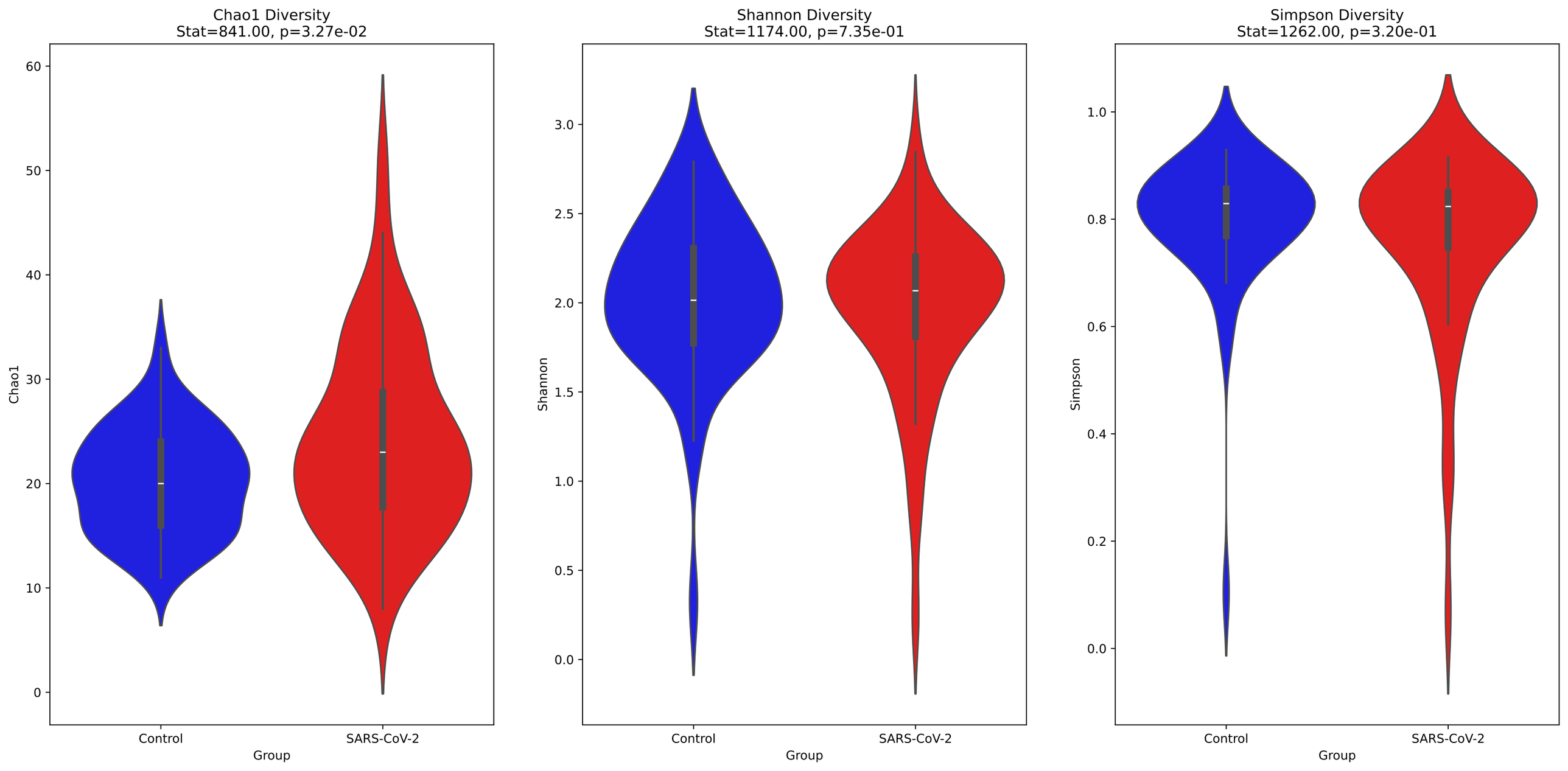
Chao1 Diversity
Stat=841.00, p=3.27e-02
Chao1
60
50
40
30
20
10
0
Control
SARS-CoV-2
Group
Shannon Diversity
Stat=1174.00, p=7.35e-01
Shannon
3.0
2.5
2.0
1.5
1.0
0.5
0.0
Control
SARS-CoV-2
Group
Simpson Diversity
Stat=1262.00, p=3.20e-01
Simpson
1.0
0.8
0.6
0.4
0.2
0.0
Control
SARS-CoV-2
Group

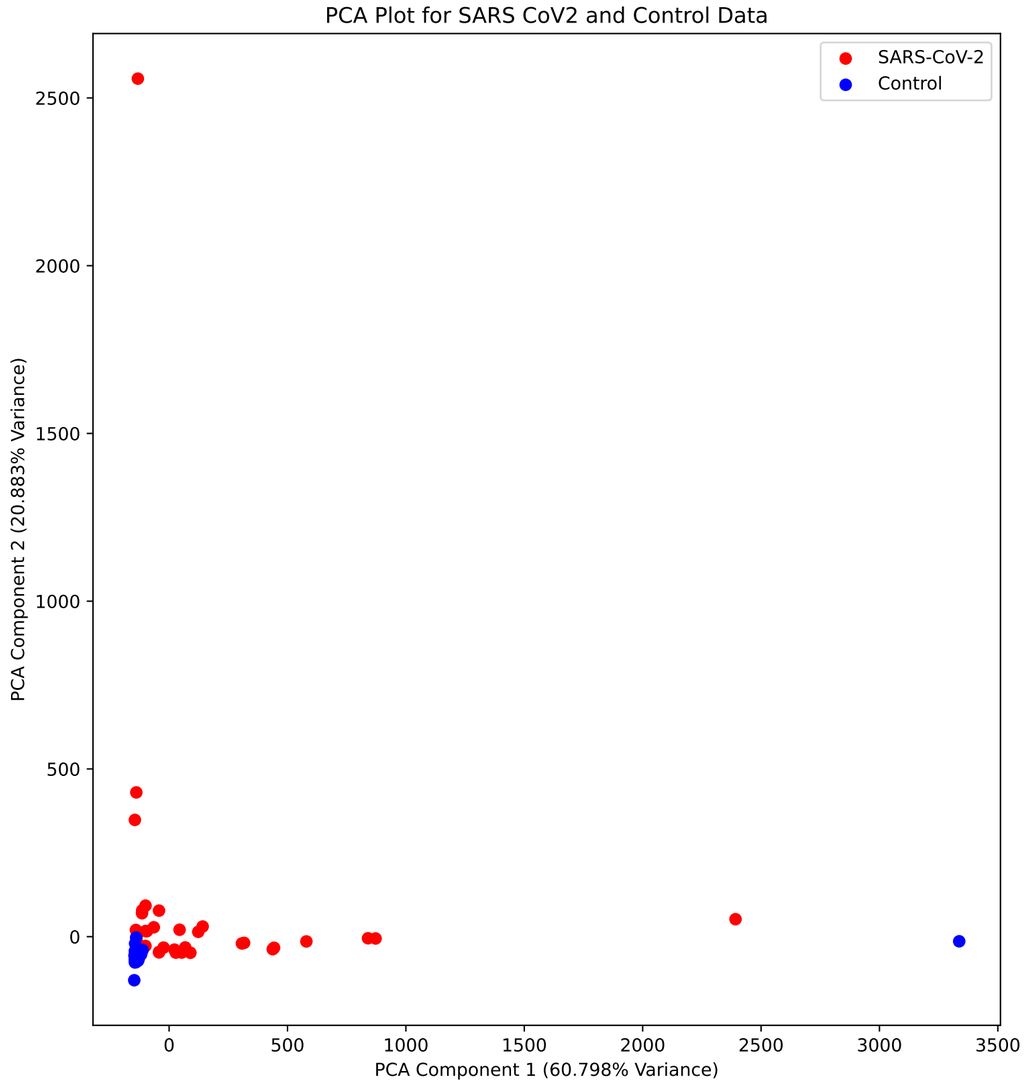
PCA Plot for SARS CoV2 and Control Data
SARS-CoV-2
Control
PCA Component 2 (20.883% Variance)
PCA Component 1 (60.798% Variance)
2500
2000
1500
1000
500
0
0
500
1000
1500
2000
2500
3000
3500

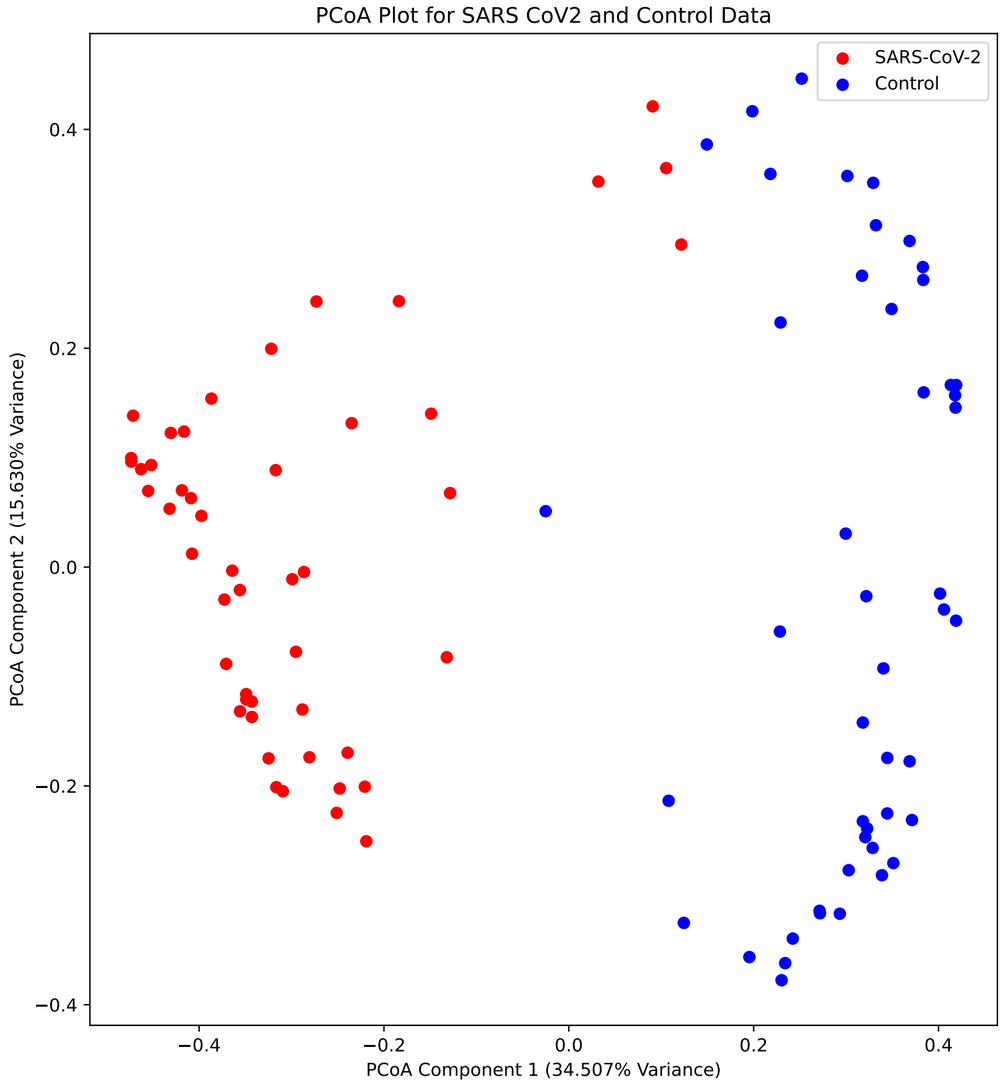
PCoA Plot for SARS CoV2 and Control Data
SARS-CoV-2
Control
PCoA Component 2 (15.630% Variance)
PCoA Component 1 (34.507% Variance)
0.4
0.2
0.0
−0.2
−0.4
−0.4
−0.2
0.0
0.2
0.4

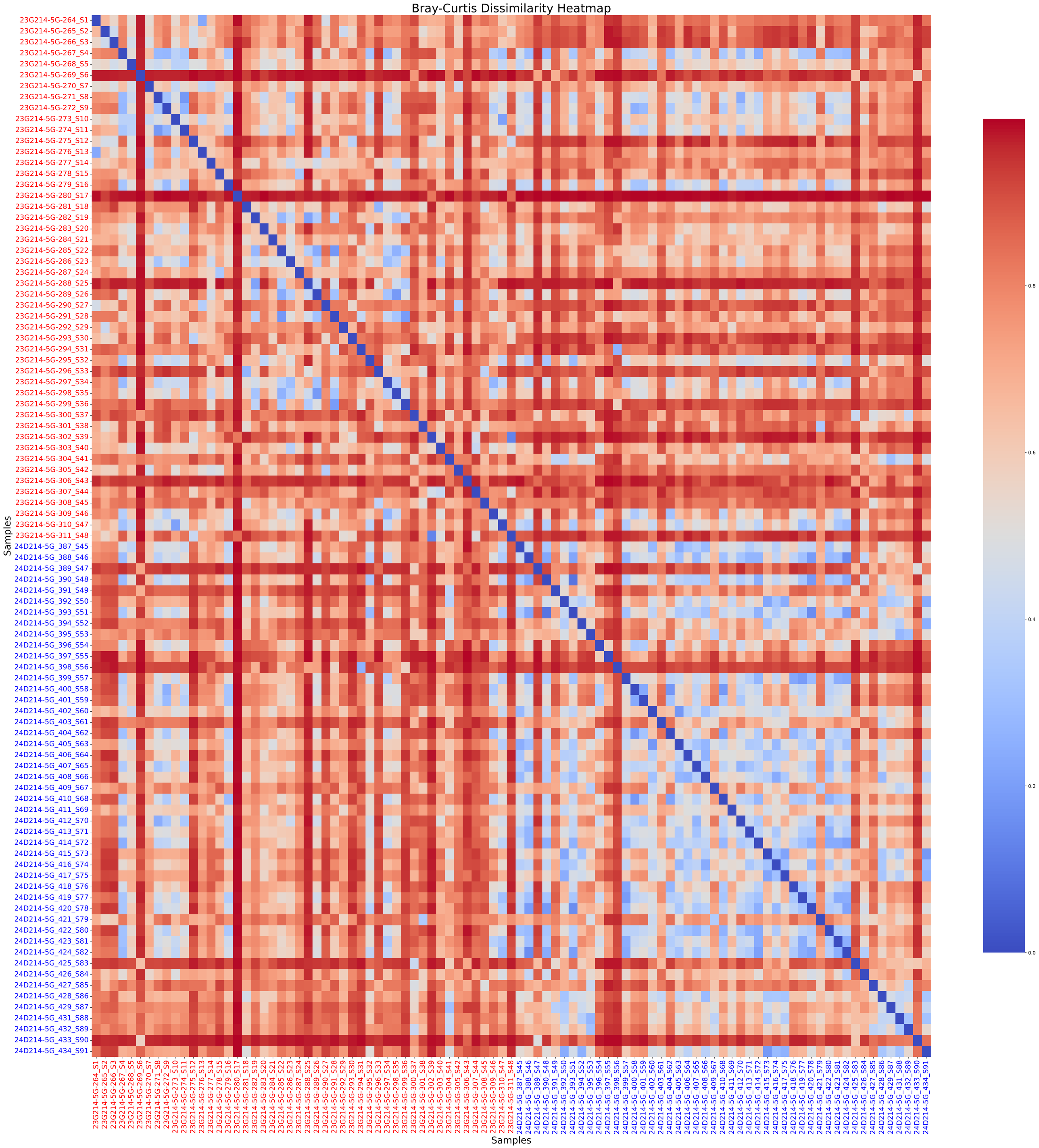
Bray-Curtis Dissimilarity Heatmap
Samples
Samples
0.8
0.6
0.4
0.2
0.0

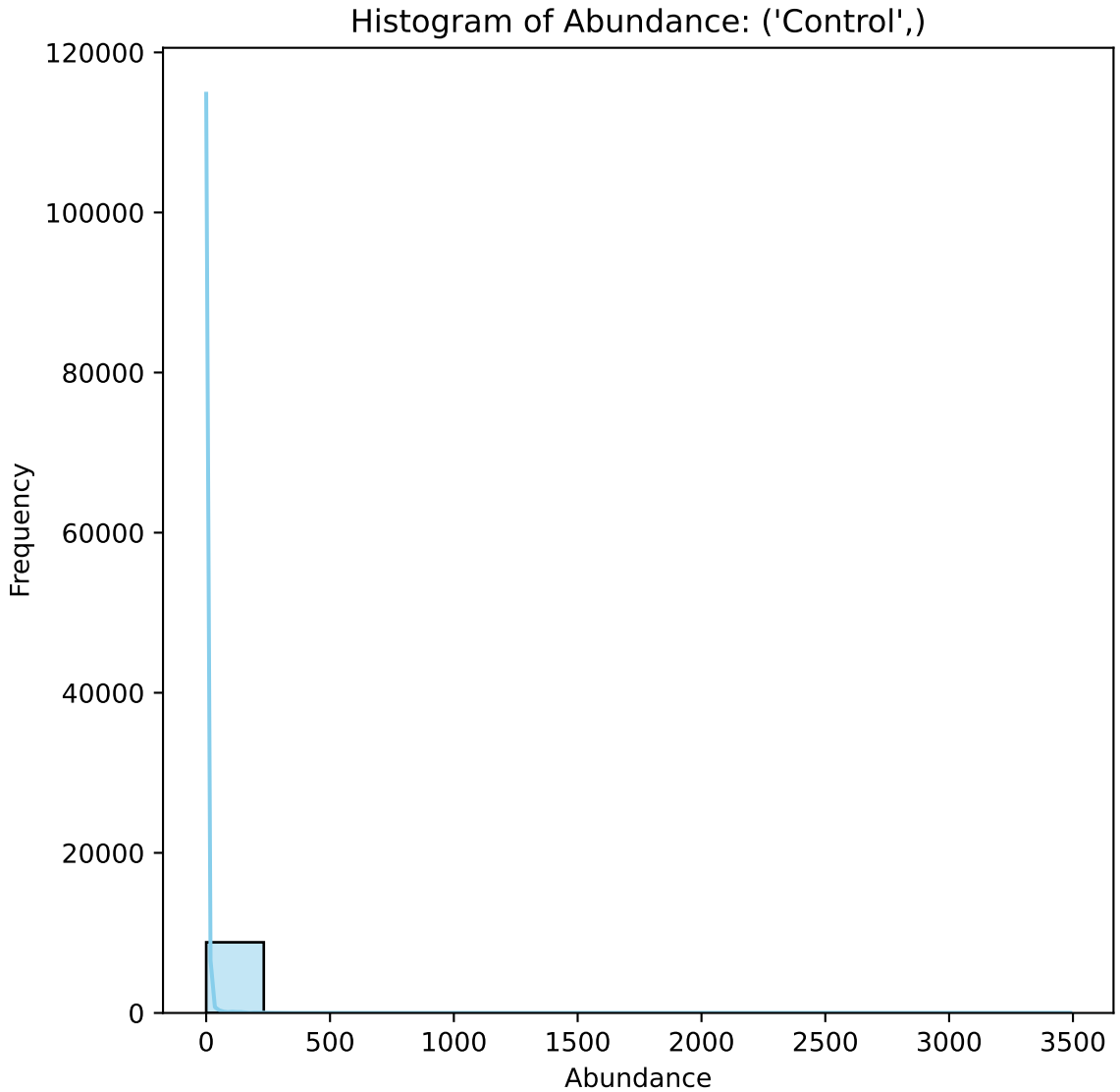
Histogram of Abundance: ('Control',)
Frequency
Abundance
0
20000
40000
60000
80000
100000
120000
0
500
1000
1500
2000
2500
3000
3500

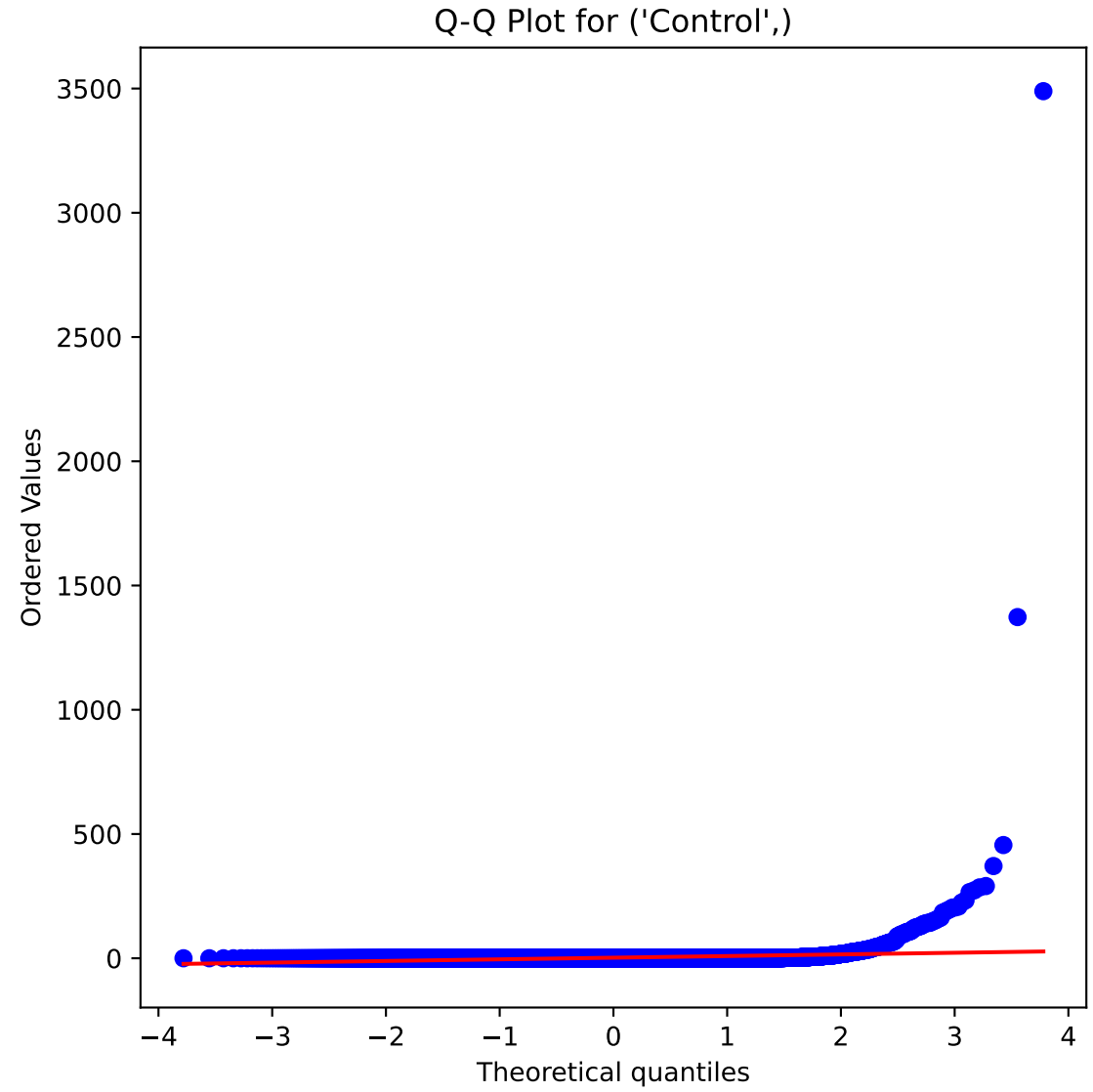
Q-Q Plot for ('Control',)
Ordered Values
Theoretical quantiles
0
500
1000
1500
2000
2500
3000
3500
−4
−3
−2
−1
0
1
2
3
4

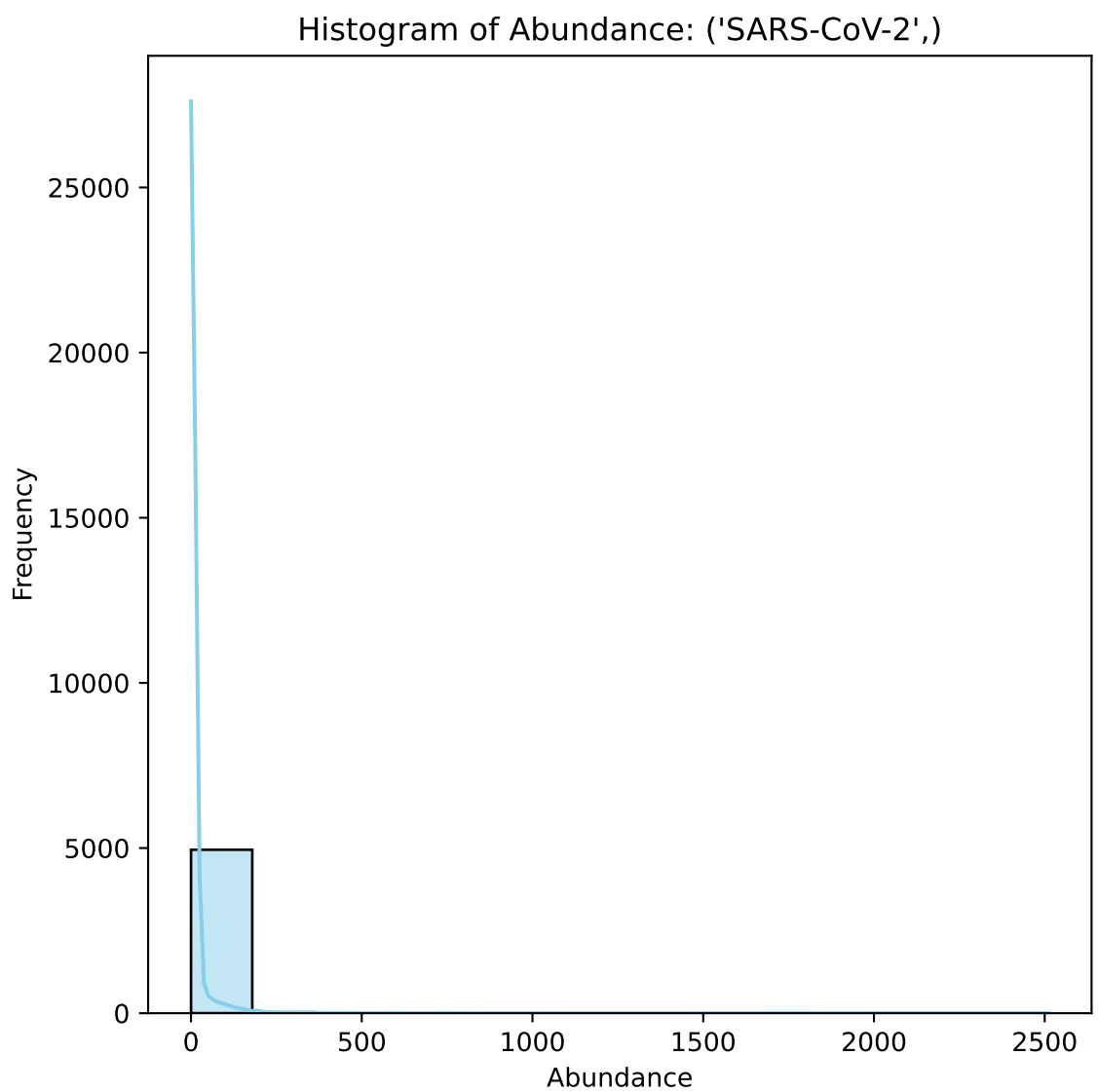
Histogram of Abundance: ('SARS-CoV-2',)
Frequency
Abundance
0
5000
10000
15000
20000
25000
0
500
1000
1500
2000
2500

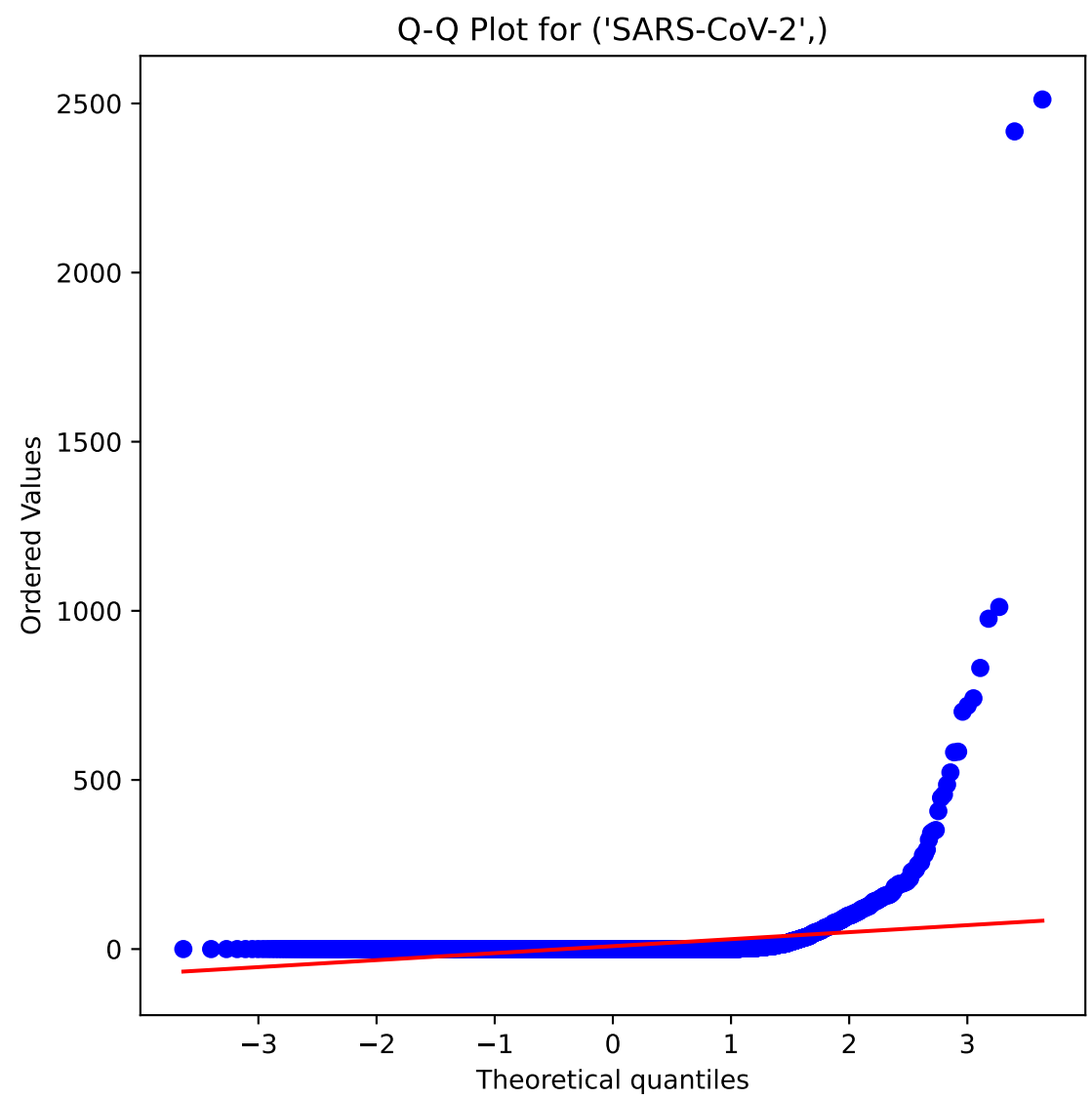
Q-Q Plot for ('SARS-CoV-2',)
Ordered Values
Theoretical quantiles
0
500
1000
1500
2000
2500
−3
−2
−1
0
1
2
3

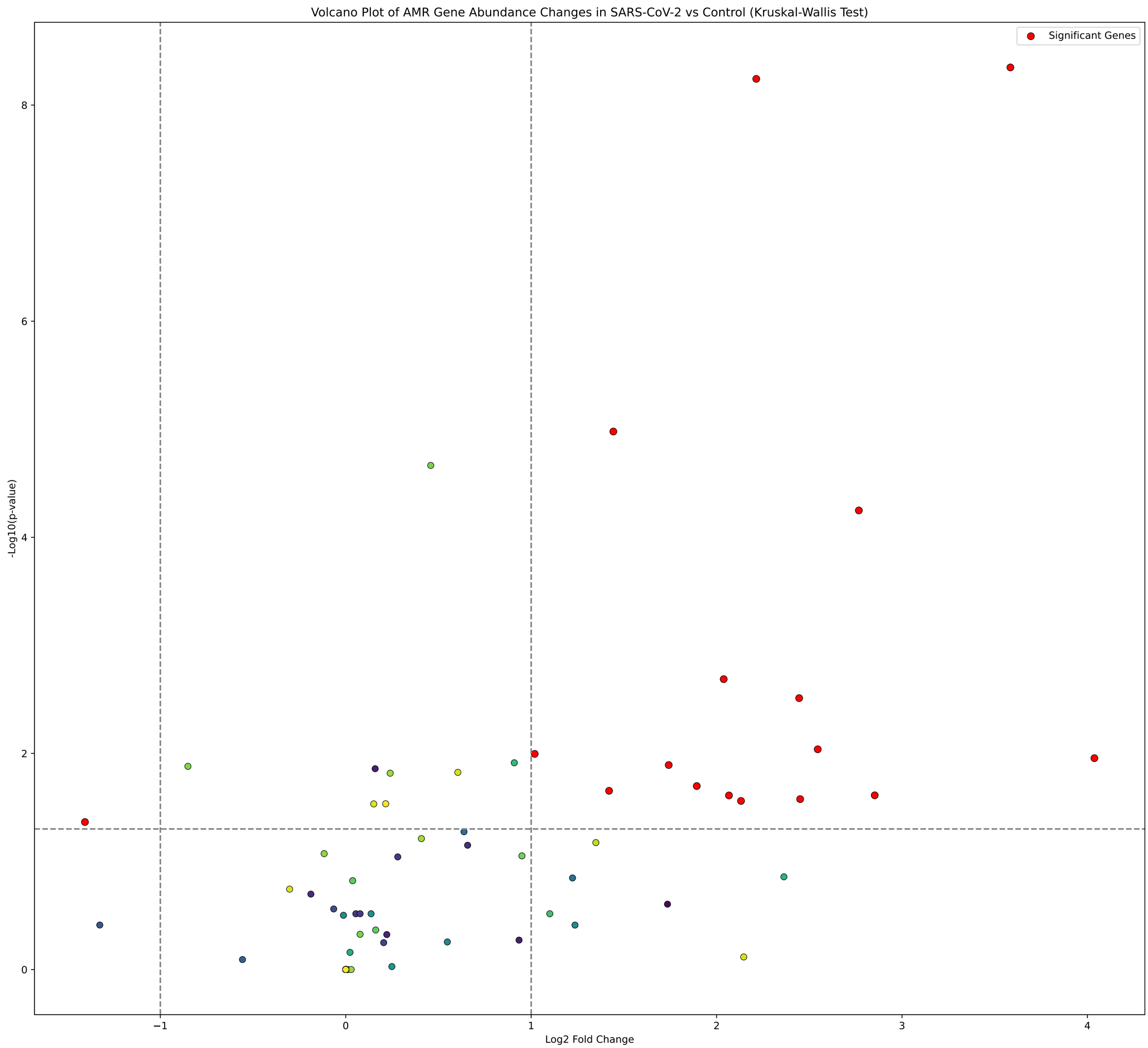
Volcano Plot of AMR Gene Abundance Changes in SARS-CoV-2 vs Control (Kruskal-Wallis Test)
Significant Genes
-Log10(p-value)
Log2 Fold Change
0
2
4
6
8
−1
0
1
2
3
4

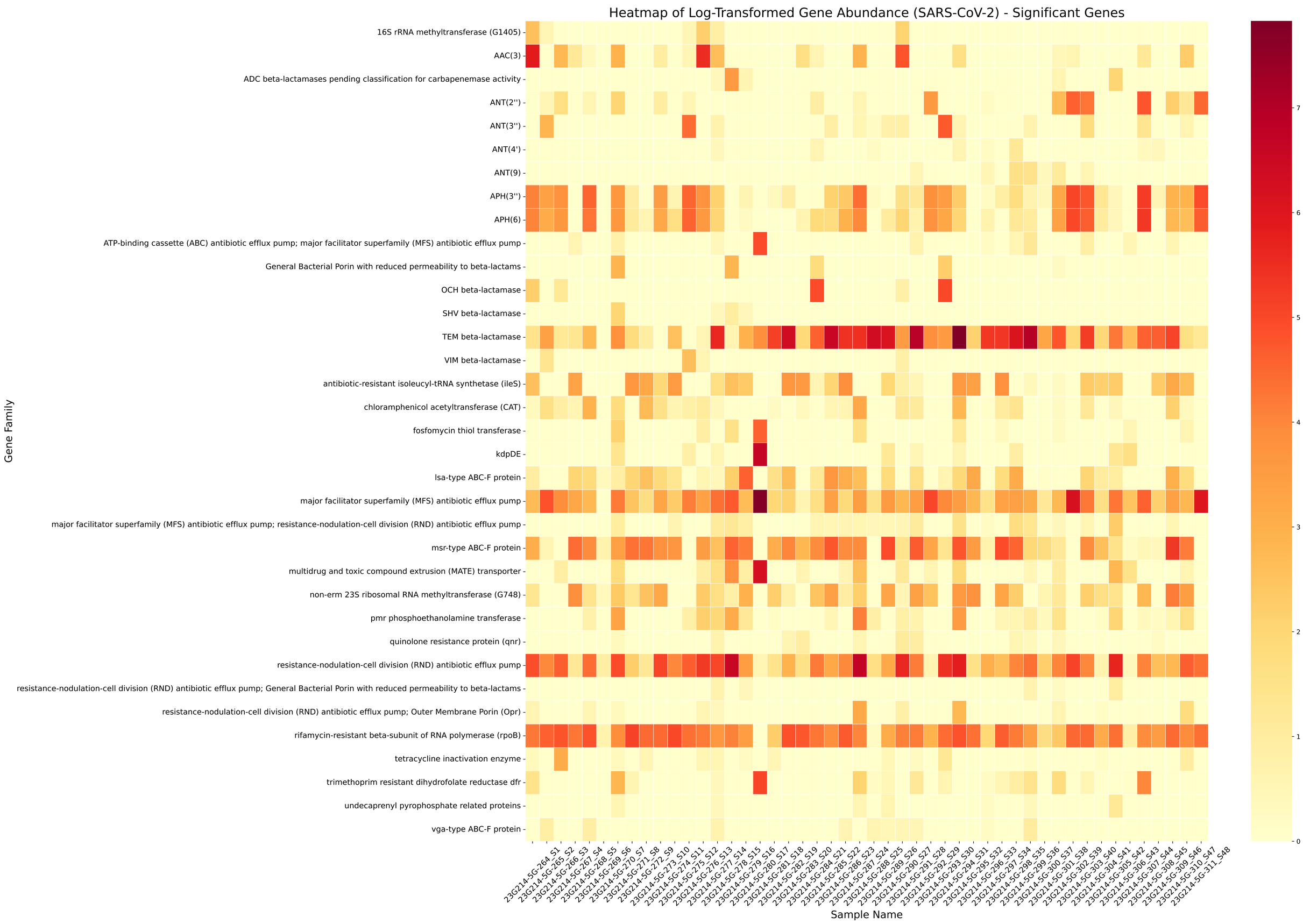
Heatmap of Log-Transformed Gene Abundance (SARS-CoV-2) - Significant Genes
Gene Family
16S rRNA methyltransferase (G1405)
AAC(3)
ADC beta-lactamases pending classification for carbapenemase activity
ANT(2'')
ANT(3'')
ANT(4')
ANT(9)
APH(3'')
APH(6)
ATP-binding cassette (ABC) antibiotic efflux pump; major facilitator superfamily (MFS) antibiotic efflux pump
General Bacterial Porin with reduced permeability to beta-lactams
OCH beta-lactamase
SHV beta-lactamase
TEM beta-lactamase
VIM beta-lactamase
antibiotic-resistant isoleucyl-tRNA synthetase (ileS)
chloramphenicol acetyltransferase (CAT)
fosfomycin thiol transferase
kdpDE
lsa-type ABC-F protein
major facilitator superfamily (MFS) antibiotic efflux pump
major facilitator superfamily (MFS) antibiotic efflux pump; resistance-nodulation-cell division (RND) antibiotic efflux pump
msr-type ABC-F protein
multidrug and toxic compound extrusion (MATE) transporter
non-erm 23S ribosomal RNA methyltransferase (G748)
pmr phosphoethanolamine transferase
quinolone resistance protein (qnr)
resistance-nodulation-cell division (RND) antibiotic efflux pump
resistance-nodulation-cell division (RND) antibiotic efflux pump; General Bacterial Porin with reduced permeability to beta-lactams
resistance-nodulation-cell division (RND) antibiotic efflux pump; Outer Membrane Porin (Opr)
rifamycin-resistant beta-subunit of RNA polymerase (rpoB)
tetracycline inactivation enzyme
trimethoprim resistant dihydrofolate reductase dfr
undecaprenyl pyrophosphate related proteins
vga-type ABC-F protein
23G214-5G-264_S1
23G214-5G-265_S2
23G214-5G-266_S3
23G214-5G-267_S4
23G214-5G-268_S5
23G214-5G-269_S6
23G214-5G-270_S7
23G214-5G-271_S8
23G214-5G-272_S9
23G214-5G-273_S10
23G214-5G-274_S11
23G214-5G-275_S12
23G214-5G-276_S13
23G214-5G-277_S14
23G214-5G-278_S15
23G214-5G-279_S16
23G214-5G-280_S17
23G214-5G-281_S18
23G214-5G-282_S19
23G214-5G-283_S20
23G214-5G-284_S21
23G214-5G-285_S22
23G214-5G-286_S23
23G214-5G-287_S24
23G214-5G-288_S25
23G214-5G-289_S26
23G214-5G-290_S27
23G214-5G-291_S28
23G214-5G-292_S29
23G214-5G-293_S30
23G214-5G-294_S31
23G214-5G-295_S32
23G214-5G-296_S33
23G214-5G-297_S34
23G214-5G-298_S35
23G214-5G-299_S36
23G214-5G-300_S37
23G214-5G-301_S38
23G214-5G-302_S39
23G214-5G-303_S40
23G214-5G-304_S41
23G214-5G-305_S42
23G214-5G-306_S43
23G214-5G-307_S44
23G214-5G-308_S45
23G214-5G-309_S46
23G214-5G-310_S47
23G214-5G-311_S48
Sample Name
0
1
2
3
4
5
6
7

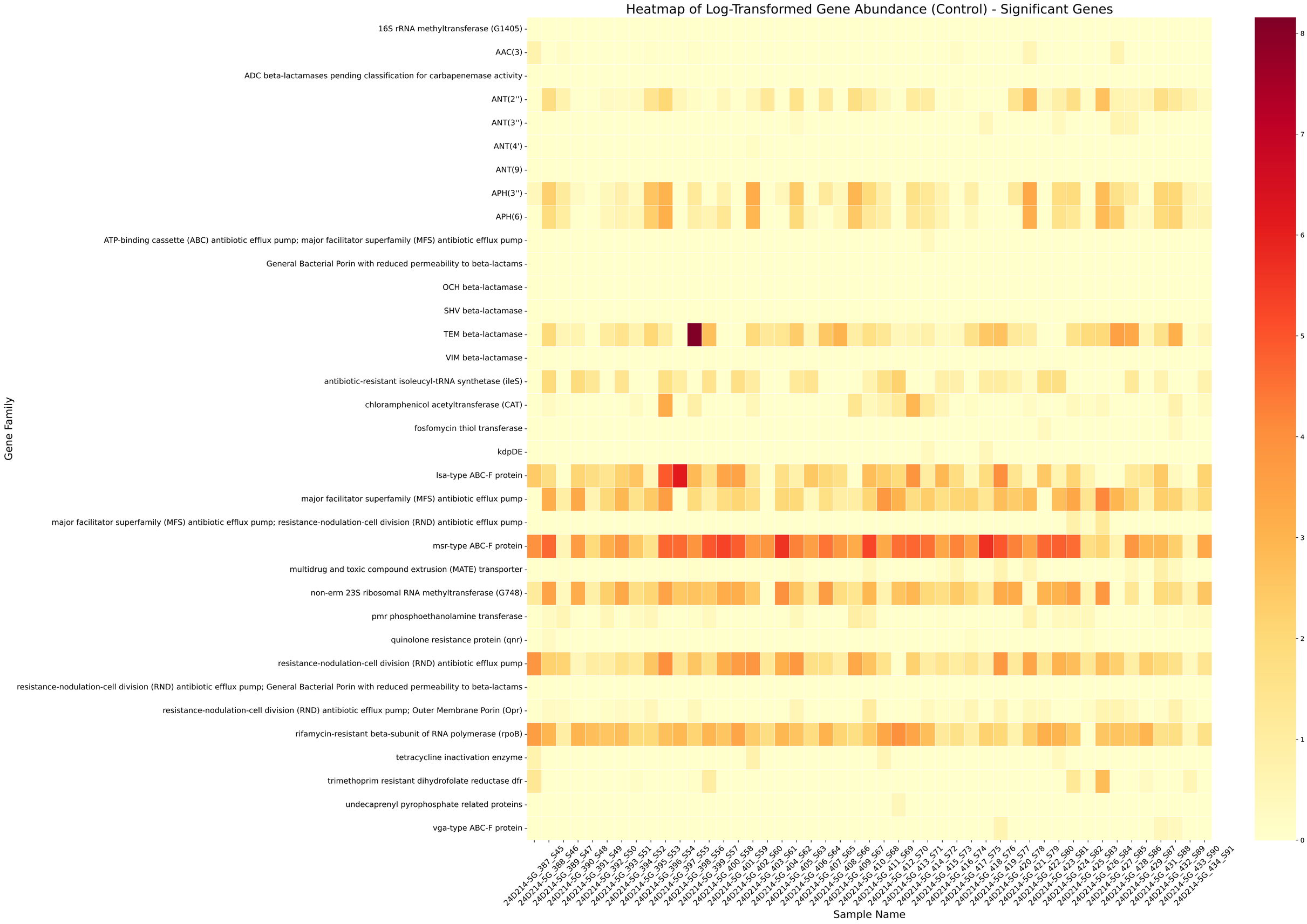
Heatmap of Log-Transformed Gene Abundance (Control) - Significant Genes
Gene Family
16S rRNA methyltransferase (G1405)
AAC(3)
ADC beta-lactamases pending classification for carbapenemase activity
ANT(2'')
ANT(3'')
ANT(4')
ANT(9)
APH(3'')
APH(6)
ATP-binding cassette (ABC) antibiotic efflux pump; major facilitator superfamily (MFS) antibiotic efflux pump
General Bacterial Porin with reduced permeability to beta-lactams
OCH beta-lactamase
SHV beta-lactamase
TEM beta-lactamase
VIM beta-lactamase
antibiotic-resistant isoleucyl-tRNA synthetase (ileS)
chloramphenicol acetyltransferase (CAT)
fosfomycin thiol transferase
kdpDE
lsa-type ABC-F protein
major facilitator superfamily (MFS) antibiotic efflux pump
major facilitator superfamily (MFS) antibiotic efflux pump; resistance-nodulation-cell division (RND) antibiotic efflux pump
msr-type ABC-F protein
multidrug and toxic compound extrusion (MATE) transporter
non-erm 23S ribosomal RNA methyltransferase (G748)
pmr phosphoethanolamine transferase
quinolone resistance protein (qnr)
resistance-nodulation-cell division (RND) antibiotic efflux pump
resistance-nodulation-cell division (RND) antibiotic efflux pump; General Bacterial Porin with reduced permeability to beta-lactams
resistance-nodulation-cell division (RND) antibiotic efflux pump; Outer Membrane Porin (Opr)
rifamycin-resistant beta-subunit of RNA polymerase (rpoB)
tetracycline inactivation enzyme
trimethoprim resistant dihydrofolate reductase dfr
undecaprenyl pyrophosphate related proteins
vga-type ABC-F protein
24D214-5G_387_S45
24D214-5G_388_S46
24D214-5G_389_S47
24D214-5G_390_S48
24D214-5G_391_S49
24D214-5G_392_S50
24D214-5G_393_S51
24D214-5G_394_S52
24D214-5G_395_S53
24D214-5G_396_S54
24D214-5G_397_S55
24D214-5G_398_S56
24D214-5G_399_S57
24D214-5G_400_S58
24D214-5G_401_S59
24D214-5G_402_S60
24D214-5G_403_S61
24D214-5G_404_S62
24D214-5G_405_S63
24D214-5G_406_S64
24D214-5G_407_S65
24D214-5G_408_S66
24D214-5G_409_S67
24D214-5G_410_S68
24D214-5G_411_S69
24D214-5G_412_S70
24D214-5G_413_S71
24D214-5G_414_S72
24D214-5G_415_S73
24D214-5G_416_S74
24D214-5G_417_S75
24D214-5G_418_S76
24D214-5G_419_S77
24D214-5G_420_S78
24D214-5G_421_S79
24D214-5G_422_S80
24D214-5G_423_S81
24D214-5G_424_S82
24D214-5G_425_S83
24D214-5G_426_S84
24D214-5G_427_S85
24D214-5G_428_S86
24D214-5G_429_S87
24D214-5G_431_S88
24D214-5G_432_S89
24D214-5G_433_S90
24D214-5G_434_S91
Sample Name
0
1
2
3
4
5
6
7
8

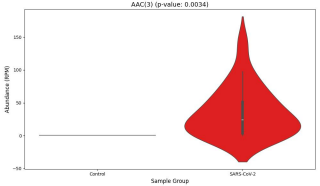
AAC(3) (p-value: 0.0034)
Abundance (RPM)
Control
SARS-CoV-2
Sample Group

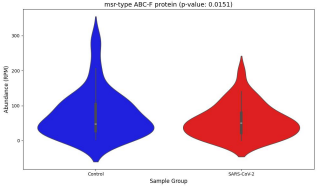
msr-type ABC-F protein (p-value: 0.0151)
Abundance (RPM)
Control
SARS-CoV-2
Sample Group

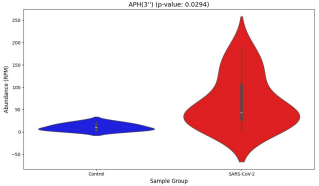
APH(3'') (p-value: 0.0294)
Abundance (RPM)
Control
SARS-CoV-2
Sample Group

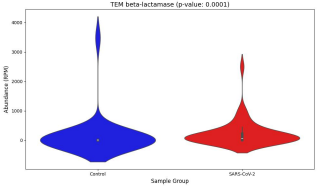
TEM beta-lactamase (p-value: 0.0001)
Abundance (RPM)
Control
SARS-CoV-2
Sample Group

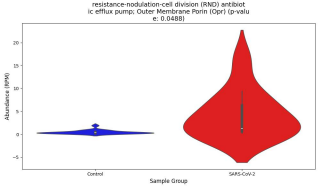
resistance-nodulation-cell division (RND) antibiot
ic efflux pump; Outer Membrane Porin (Opr) (p-valu
e: 0.0488)
Abundance (RPM)
Control
SARS-CoV-2
Sample Group

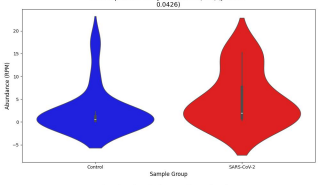
chloramphenicol acetyltransferase (CAT) (p-value:
0.0426)
Abundance (RPM)
Control
SARS-CoV-2
Sample Group

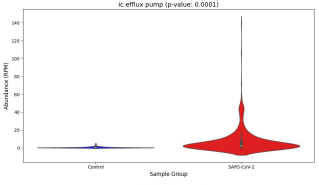
resistance-nodulation-cell division (RND) antibiot
ic efflux pump (p-value: 0.0001)
Abundance (RPM)
Control
SARS-CoV-2
Sample Group

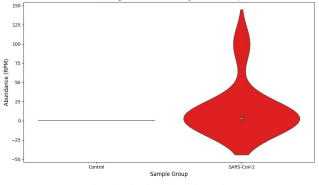
fosfomycin thiol transferase (p-value: 0.0130)
Abundance (RPM)
Control
SARS-CoV-2
Sample Group

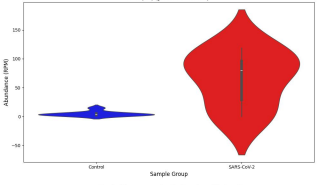
ANT(2'') (p-value: 0.0203)
Abundance (RPM)
Control
SARS-CoV-2
Sample Group

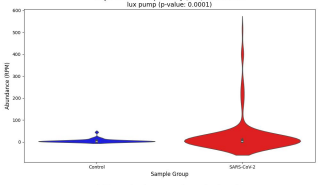
major facilitator superfamily (MFS) antibiotic eff
lux pump (p-value: 0.0001)
Abundance (RPM)
Control
SARS-CoV-2
Sample Group

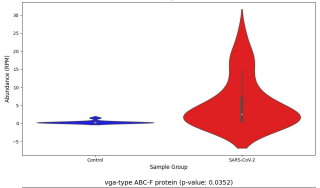
pmr phosphoethanolamine transferase (p-value: 0.01
71)
Abundance (RPM)
Control
SARS-CoV-2
Sample Group

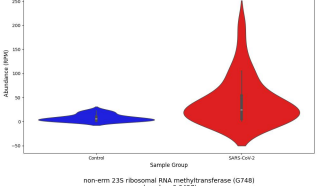
APH(6) (p-value: 0.0095)
Abundance (RPM)
Control
SARS-CoV-2
Sample Group

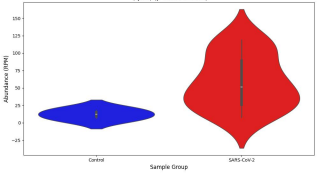
rifamycin-resistant beta-subunit of RNA polymerase
(rpoB) (p-value: 0.0001)
Abundance (RPM)
Control
SARS-CoV-2
Sample Group

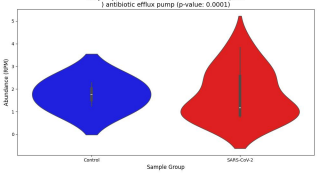
major facilitator superfamily (MFS) antibiotic eff
lux pump; resistance-nodulation-cell division (RND
) antibiotic efflux pump (p-value: 0.0001)
Abundance (RPM)
Control
SARS-CoV-2
Sample Group

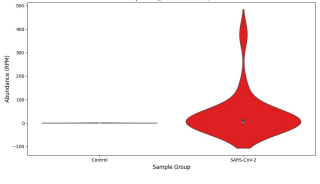
multidrug and toxic compound extrusion (MATE) tran
sporter (p-value: 0.0253)
Abundance (RPM)
Control
SARS-CoV-2
Sample Group

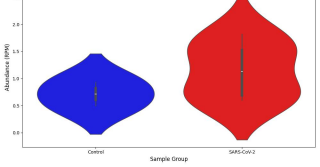
vga-type ABC-F protein (p-value: 0.0352)
Abundance (RPM)
Control
SARS-CoV-2
Sample Group

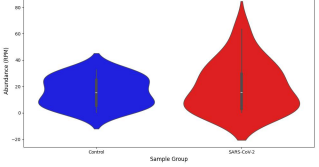
non-erm 23S ribosomal RNA methyltransferase (G748)
(p-value: 0.0427)
Abundance (RPM)
Control
SARS-CoV-2
Sample Group

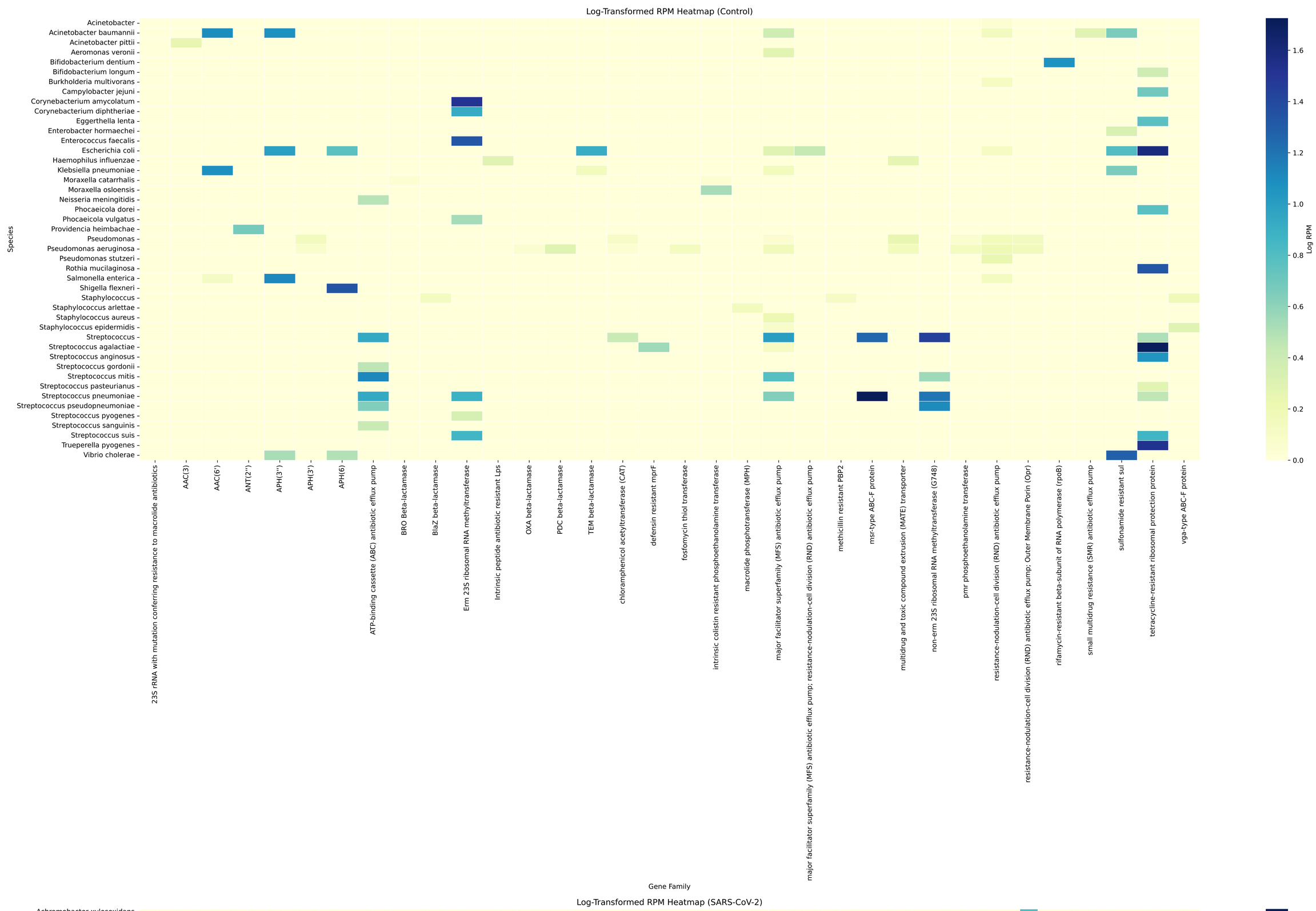
Log-Transformed RPM Heatmap (Control)
Species
Gene Family
Log RPM
Acinetobacter
Acinetobacter baumannii
Acinetobacter pittii
Aeromonas veronii
Bifidobacterium dentium
Bifidobacterium longum
Burkholderia multivorans
Campylobacter jejuni
Corynebacterium amycolatum
Corynebacterium diphtheriae
Eggerthella lenta
Enterobacter hormaechei
Enterococcus faecalis
Escherichia coli
Haemophilus influenzae
Klebsiella pneumoniae
Moraxella catarrhalis
Moraxella osloensis
Neisseria meningitidis
Phocaeicola dorei
Phocaeicola vulgatus
Providencia heimbachae
Pseudomonas
Pseudomonas aeruginosa
Pseudomonas stutzeri
Rothia mucilaginosa
Salmonella enterica
Shigella flexneri
Staphylococcus
Staphylococcus arlettae
Staphylococcus aureus
Staphylococcus epidermidis
Streptococcus
Streptococcus agalactiae
Streptococcus anginosus
Streptococcus gordonii
Streptococcus mitis
Streptococcus pasteurianus
Streptococcus pneumoniae
Streptococcus pseudopneumoniae
Streptococcus pyogenes
Streptococcus sanguinis
Streptococcus suis
Trueperella pyogenes
Vibrio cholerae
23S rRNA with mutation conferring resistance to macrolide antibiotics
AAC(3)
AAC(6')
ANT(2'')
APH(3'')
APH(3')
APH(6)
ATP-binding cassette (ABC) antibiotic efflux pump
BRO Beta-lactamase
BlaZ beta-lactamase
Erm 23S ribosomal RNA methyltransferase
Intrinsic peptide antibiotic resistant Lps
OXA beta-lactamase
PDC beta-lactamase
TEM beta-lactamase
chloramphenicol acetyltransferase (CAT)
defensin resistant mprF
fosfomycin thiol transferase
intrinsic colistin resistant phosphoethanolamine transferase
macrolide phosphotransferase (MPH)
major facilitator superfamily (MFS) antibiotic efflux pump
major facilitator superfamily (MFS) antibiotic efflux pump; resistance-nodulation-cell division (RND) antibiotic efflux pump
methicillin resistant PBP2
msr-type ABC-F protein
multidrug and toxic compound extrusion (MATE) transporter
non-erm 23S ribosomal RNA methyltransferase (G748)
pmr phosphoethanolamine transferase
resistance-nodulation-cell division (RND) antibiotic efflux pump
resistance-nodulation-cell division (RND) antibiotic efflux pump; Outer Membrane Porin (Opr)
rifamycin-resistant beta-subunit of RNA polymerase (rpoB)
small multidrug resistance (SMR) antibiotic efflux pump
sulfonamide resistant sul
tetracycline-resistant ribosomal protection protein
vga-type ABC-F protein
0.0
0.2
0.4
0.6
0.8
1.0
1.2
1.4
1.6
Log-Transformed RPM Heatmap (SARS-CoV-2)
Species
Gene Family
Log RPM
Achromobacter xylosoxidans
Acinetobacter
Acinetobacter baumannii
Acinetobacter haemolyticus
Acinetobacter johnsonii
Acinetobacter pittii
Bifidobacterium animalis
Bifidobacterium breve
Bifidobacterium dentium
Bifidobacterium longum
Brucella intermedia
Campylobacter coli
Citrobacter
Citrobacter amalonaticus
Citrobacter freundii
Collinsella aerofaciens
Corynebacterium diphtheriae
Corynebacterium urealyticum
Eggerthella lenta
Enterobacter
Enterobacter cloacae
Enterobacter hormaechei
Enterococcus faecalis
Escherichia
Escherichia coli
Faecalibacterium prausnitzii
Fusobacterium nucleatum
Haemophilus influenzae
Klebsiella
Klebsiella michiganensis
Klebsiella pneumoniae
Klebsiella quasipneumoniae
Micrococcus luteus
Moraxella catarrhalis
Moraxella osloensis
Neisseria meningitidis
Nocardia farcinica
Paracoccus denitrificans
Pasteurella multocida
Porphyromonas gingivalis
Proteus mirabilis
Providencia heimbachae
Pseudomonas
Pseudomonas aeruginosa
Pseudomonas mendocina
Pseudomonas putida
Pseudomonas stutzeri
Ralstonia mannitolilytica
Rothia mucilaginosa
Salmonella enterica
Shigella sonnei
Sphingobium yanoikuyae
Staphylococcus
Staphylococcus arlettae
Staphylococcus aureus
Staphylococcus epidermidis
Staphylococcus haemolyticus
Staphylococcus hominis
Staphylococcus lugdunensis
Staphylococcus warneri
Stenotrophomonas maltophilia
Streptococcus
Streptococcus cristatus
Streptococcus gordonii
Streptococcus gwangjuense
Streptococcus mitis
Streptococcus mutans
Streptococcus pneumoniae
Streptococcus pseudopneumoniae
Streptococcus pyogenes
Streptococcus sanguinis
Streptococcus suis
Thalassospira indica
Vibrio
Vibrio cholerae
Vibrio parahaemolyticus
16S rRNA methyltransferase (G1405)
AAC(3)
AAC(6')
ACT beta-lactamase
ADC beta-lactamase without carbapenemase activity
ADC beta-lactamases pending classification for carbapenemase activity
ANT(2'')
ANT(3'')
APH(3'')
APH(3')
APH(6)
ARL Beta-lactamase
ATP-binding cassette (ABC) antibiotic efflux pump
ATP-binding cassette (ABC) antibiotic efflux pump; major facilitator superfamily (MFS) antibiotic efflux pump
ATP-binding cassette (ABC) antibiotic efflux pump; major facilitator superfamily (MFS) antibiotic efflux pump; resistance-nodulation-cell division (RND) antibiotic efflux pump
BRO Beta-lactamase
BlaZ beta-lactamase
Bleomycin resistant protein
CARB beta-lactamase
EC beta-lactamase
Erm 23S ribosomal RNA methyltransferase
General Bacterial Porin with reduced permeability to beta-lactams
General Bacterial Porin with reduced permeability to peptide antibiotics
Intrinsic peptide antibiotic resistant Lps
OXA beta-lactamase
OXY beta-lactamase
PDC beta-lactamase
PRC beta-lactamase
SHV beta-lactamase
TEM beta-lactamase
Target protecting FusB-type protein conferring resistance to Fusidic acid
VIM beta-lactamase
aminoglycoside bifunctional resistance protein
antibiotic-resistant isoleucyl-tRNA synthetase (ileS)
chloramphenicol acetyltransferase (CAT)
fosfomycin thiol transferase
intrinsic colistin resistant phosphoethanolamine transferase
kdpDE
lipid A acyltransferase; polymyxin resistance operon
lipid A phosphatase
macrolide phosphotransferase (MPH)
major facilitator superfamily (MFS) antibiotic efflux pump
major facilitator superfamily (MFS) antibiotic efflux pump; resistance-nodulation-cell division (RND) antibiotic efflux pump
methicillin resistant PBP2
msr-type ABC-F protein
multidrug and toxic compound extrusion (MATE) transporter
non-erm 23S ribosomal RNA methyltransferase (G748)
pmr phosphoethanolamine transferase
quinolone resistance protein (qnr)
resistance-nodulation-cell division (RND) antibiotic efflux pump
resistance-nodulation-cell division (RND) antibiotic efflux pump; General Bacterial Porin with reduced permeability to beta-lactams
resistance-nodulation-cell division (RND) antibiotic efflux pump; Outer Membrane Porin (Opr)
rifamycin-resistant beta-subunit of RNA polymerase (rpoB)
small multidrug resistance (SMR) antibiotic efflux pump
sulfonamide resistant sul
tetracycline-resistant ribosomal protection protein
trimethoprim resistant dihydrofolate reductase dfr
undecaprenyl pyrophosphate related proteins
vga-type ABC-F protein
0.0
0.5
1.0
1.5
2.0

Sankey Diagram: Control (Thickness by RPM)

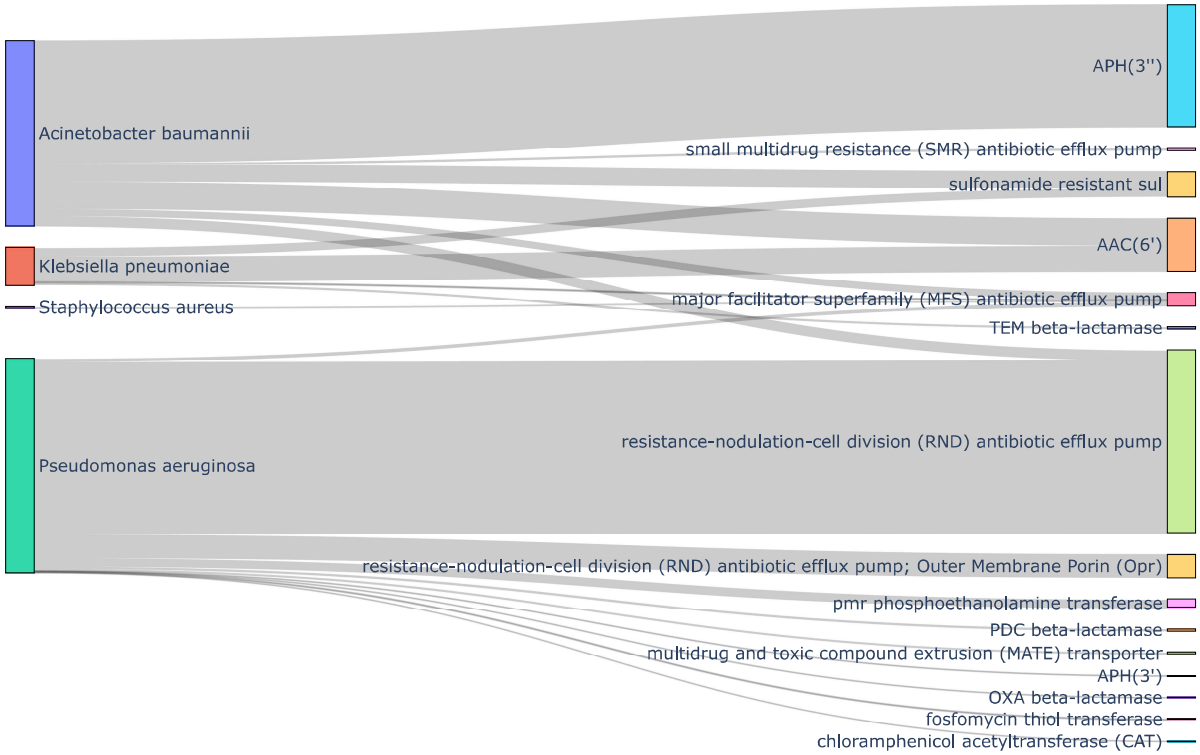
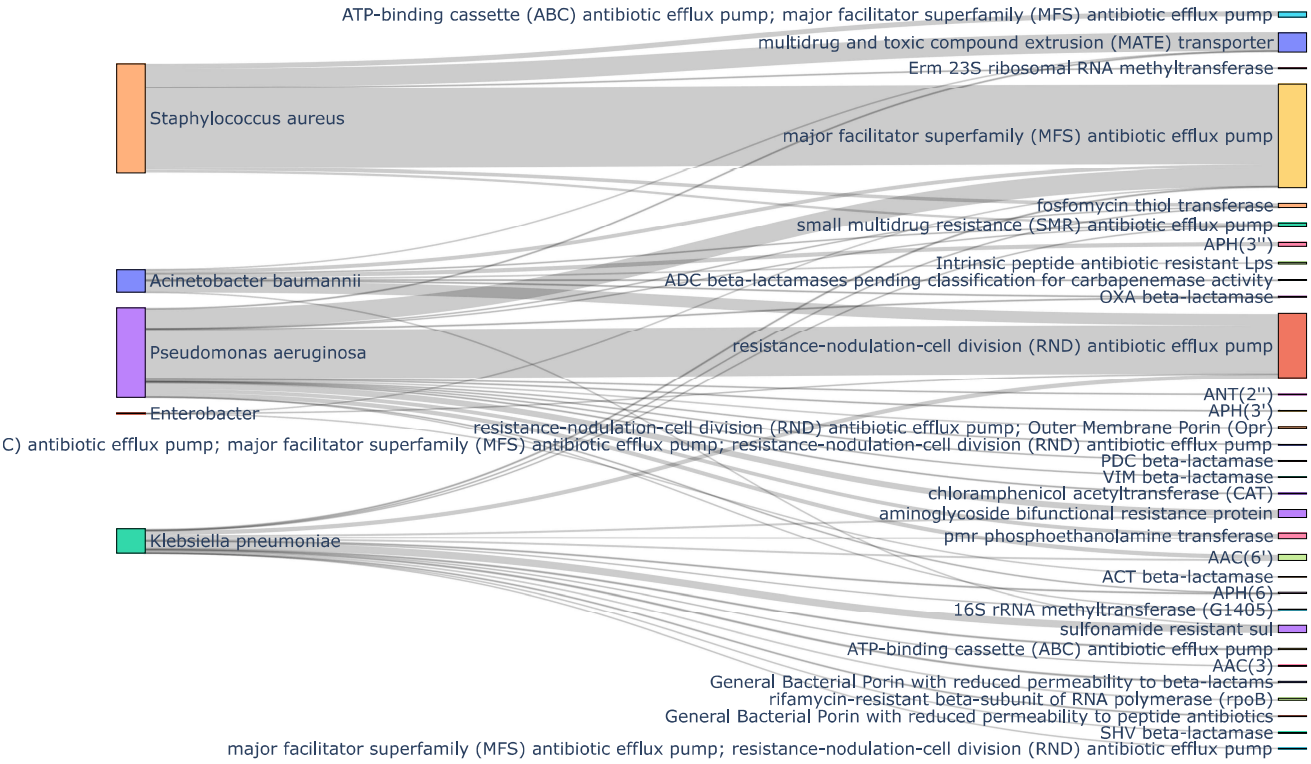
Sankey Diagram: SARS-CoV-2 (Thickness by RPM)